Journal of Environmental Chemical Engineering 12 (2024) 111861

Contents lists available at ScienceDirect

Journal of Environmental Chemical Engineering

journal homepage: www.elsevier.com/locate/jece

Di-imine Schiff base inhibitor for carbon steel corrosion in 1 M HCl: Electrochemical, surface and theoretical investigations

A. Elaraby [a,b,*], Khaled Faisal Qasim [a,**], Shaimaa K. Mohamed [a], E.A. El-Sharkawy [a], Samar Abdelhamed [c]

[a] Department of Chemistry, Faculty of Science, Suez University, Suez, Egypt
[b] Egyptian Petroleum Research Institute, Nasr City 11727, Cairo, Egypt
[c] Department of Basic Science, Faculty of Engineering at Shoubra, Benha University, Egypt

ARTICLE INFO

Editor: Apostolos Giannis

Keywords:
Schiff base
Carbon steel
Adsorption
SEM
DFT

ABSTRACT

Many strategies for an efficient inhibitor preparing were proposed for metals protection against corrosion in last decades. Herein, the adsorption and inhibitory effect of aromatic di-imine Schiff base inhibitor (*Ar-Sb*) namely (N1-(2-(((E)− 4-(dimethylamino)benzylidene)amino)ethyl)-N2-(2-((2-((2(Z)− 4-dimethylamino)ben- zylidene) amino) ethyl) amino) ethyl) amino) ethyl)ethane-1,2-diamine) on carbon steel (*CS*) in 1 M HCl solution was investigated experimentally and theoretically. The electrochemical measurements (EMs) such as electrochemical impedance spectroscopy (EIS), Potentiodynamic polarization (PDP) and cyclic voltammetry (CV) techniques exhibited the anticorrosion performance of *Ar-Sb*. Also, the adsorption of *Ar-Sb* on *CS* surface at different temperatures and immersion times was studied using PDP and EIS which indicated formation of a protective film layer of *Ar-Sb* responsible for *CS* corrosion mitigation. *Ar-Sb* inhibitor provided 95.79% inhibition efficiency at 5 $\times$ 10^{-4} M which reflected blocking of *CS* active sites through the adsorption process which was studied using various adsorption isotherms. *CS* surface morphology was studied using scanning electron microscopy (SEM), energy dispersive X-ray (EDX) and atomic force microscope (AFM) reflecting the inhibition role of *Ar-Sb* in *CS* protection. The data obtained from PDP suggested that *Ar-Sb* inhibitor acted as mixed-type inhibitor. Also, quantum calculations such as density functional theory (DFT) and Monte Carlo (MCs) verified the inhibitive performance of *Ar-Sb* for *CS* surface with the experimental results.

1. Introduction

Carbon steel (*CS*) is carbon-iron alloy with appreciable quantities of other elements [1,2]. It represents the most substantial and backbone material in several industries from high-tech devices and machinery to large-scale industrial productions such as auto parts, pipelines, buildings, heat exchangers, boilers, and numerous mechanical applications due to its high economic value and physical-mechanical properties [3]. Although the numerous applications of *CS* in different industrial fields and its properties and high qualities, it suffering from corrosion process occurred during industry [4–7]. The use of acids in the industry in descaling and oil well acidizing leads to gradual dissolution of the metal. The dissolution of metal can be minimized by surface metal modification or by making the surrounding environment of the exposed metal less severe or destructive [8]. One of the most effective methods in corrosion protection is the utilizing of corrosion inhibitors (CI_S) [9–11]. CI_S reduce *CS* dissolution rate after the addition of small quantities of CI_S which decrease the contact between *CS* and corrosive surrounding environment [12–14]. CI_S protect *CS* from corrosion by formation of a protective barrier layer over *CS* surface through their adsorption process via their active groups [15–17]. The adsorption of CI_S can occur chemically by formation of coordination bond with the vacant Fe 3d-orbital or physically through electrostatic cuteness between charged *CS* surface and charged CI_S [18,19]. The mitigation and adsorption capacity of CI_S depend on their chemical and electronic structure besides surface nature and corrosive particles[20]. Organic inhibitors augmented with hetero atoms (N, O, S or P), π-bond, and aromatic rings are more adsorbed and effective inhibitors [21]. So, in last decades, scientists focused in finding an efficient and low-cost technique for *CS* protection to reduce the high cost resulted from corrosion process in various hostile media such as

* Corresponding author at: Department of Chemistry, Faculty of Science, Suez University, Suez, Egypt.
** Corresponding author.
E-mail addresses: a_elaraby19@yahoo.com (A. Elaraby), Khaled_faisal92@hotmail.com (K.F. Qasim).

https://doi.org/10.1016/j.jece.2023.111861
Received 14 November 2023; Received in revised form 22 December 2023; Accepted 30 December 2023
Available online 3 January 2024

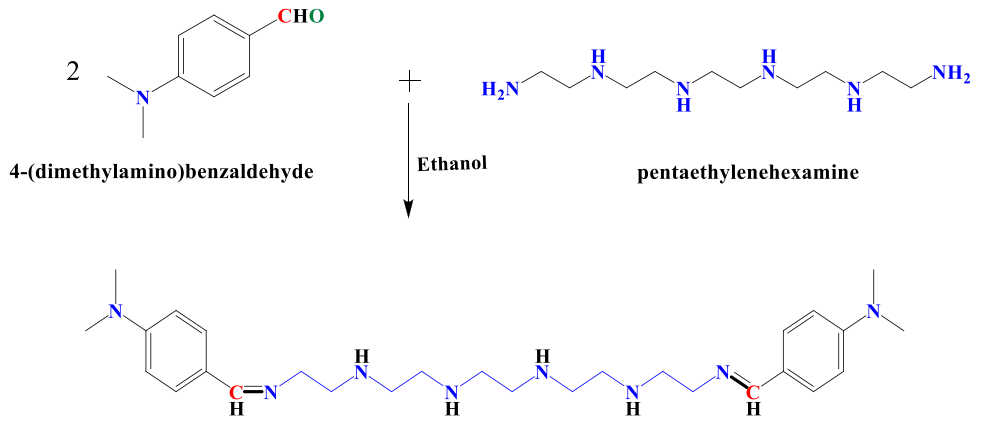

Scheme 1. synthesis of *Ar-Sb* inhibitor.

nitrate, sulfate and chloride solutions. Several studies have reported that derivatives of Schiff bases are potentially eco-friendly corrosion inhibitors in different media[22,23]. The effectiveness of Schiff bases as corrosion inhibitors may be attributed to the ability to donate unshared electron pair from N atom and form complexes at the metal surface[8]. Organic inhibitors based on Schiff bases (*Sb*) are widely used due to their easily preparation, low cost and toxicity, eco-friendly and presence of azomethine group (–C═N–) besides many of the above features which make them a promising effective CI_S [24]. These characteristics allow *Sb* inhibitors to cover *CS* surface forming a barrier layer between *CS* and the corrosive surrounding through the adsorption process[19]. Salim et.al. [25] studied the *CS* corrosion protection in 0.1 M HCl solution using SB-CH_3 and SB–OCH_3 as *Sb* corrosion inhibitors which was confirmed via electrochemical techniques and found that their mitigation potency was 91.29% and 92.20% for SB-CH_3 and SB–OCH_3 respectively based on electrochemical impedance spectroscopy (EIS). Murmu et.al.[26] investigated the inhibition performance of a pair of Sb inhibitors (PMP and PPMP) for *CS* in 1 M HCl through gravimetric and electrochemical measurements. Their inhibition efficiency increased till reach 88.89% and 93% for PMP and PPMP respectively. Li et.al.[27] studied the mitigation effect of two double Schiff bases (PAMP and PPM) for *CS* in 1 M HCl electrolyte and showed that their efficiency was 87.24% and 92.95% in presence of PAMP and PPM respectively.

In the present study, aromatic di-imine Schiff base inhibitor (*Ar-Sb*) abundant with double C═N, hetero atom (N-atom), and two aromatic rings was easy produced in one simple step (condensation reaction) which displays a good solubility in polar solvent, such as water, methanol, ethanol and acetone. *Ar-Sb* was applied as corrosion inhibitor for *CS* in 1 M HCl solution. The mitigation effect of *Ar-Sb* was evaluated using electrochemical impedance spectroscopy (EIS), Potentiodynamic polarization (PDP) and cyclic voltammetry (CV) techniques. Also, the adsorption power and anti-corrosion performance of *Ar-Sb* at various temperature range and immersion times was studied using electrochemical measurements (EMs). *CS* surface was also analyzed using scanning electron microscope (SEM), energy dispersive X-ray (EDX) and atomic force microscope (AFM) for more information about the inhibition mechanism of *Ar-Sb*. Finally, the corrosion protection of *CS* surface using *Ar-Sb* was investigated using density functional theory (DFT) and Monte Carlo simulation (MCs).

2. Experimental methods

2.1. Synthesis of inhibitor

According to Scheme 1, the newly aromatic di-imine Schiff base inhibitor (*Ar-Sb*) utilized in the present study was prepared by reaction of (0.01 M) pentaethylenehexamine and (0.02 M) 4-(dimethylamino) benzaldehyde in existence of ethanol as a solvent for 8 h. The reaction mixture was cooled and the solvent was evaporated then washed using diethyl ether for achieving the prepared *Ar-Sb* as a reddish-brown semisolid. *Ar-Sb* chemical structure was confirmed by the help of IR spectrometer (Nicolet iS10) and presented in Fig. 1Si showing bands at 3367.14 cm^{-1} (νN-H stretching), 3079.21 cm^{-1} (νC-H aromatic stretching), 2902.06 cm^{-1} and 2817.2 cm^{-1} (νC-H aliphatic chain), 1606.37 cm^{-1} (νC═N), 1526.00 cm^{-1} (νC═C aromatic stretching), 1445.03 cm^{-1} (ν-CH_2 bending). ^{1}HNMR spectra of *Ar-Sb* was characterized by Switzerland, Bruker Avance as represented in Fig. 2Si δ (ppm): 1.95 (s, 4 H, CH_2N**H**CH_2), 2.42 (t, 12 H, CH_2 NHC**H**$_2$C**H**$_2$NH), 3.9 (t, 4 H, CNCH_2C**H**$_2$NH), 3.48 (s, 12 H, C**H**$_3$), 3.78 (t, 4 H, CNC**H**$_2$) and 7.01 – 7.85 (d, 8 H, C_5**H**$_4$), 8.3 (s, 2 H, **CH**═N).

2.2. Carbon steel composition and electrolytes

CS ingredients (wt%) are: (C: 0.078, Cr: 0.015, Si: 0.058, P: 0.005, Mn: 0.751, and Fe balanced). *CS* surface was treated using different grades of emery papers (400–2500) to a mirror image then washed using CH_3COCH_3 and purified H_2O before each experiment. A stock solution (1×10^{-2} M) of the synthesized *Ar-Sb* in 1 M HCl and series solutions (5×10^{-4}: 5×10^{-6}) were prepared via dilution at room temperature (20 °C ± 1 °C).

2.3. Electrochemical measurements

The electrochemical attitude of *CS* in aggressive solution of HCl free and containing various concentrations of *Ar-Sb* was studied using EIS and PDP techniques using Potentiostat/Galvanostat (Origalys) in presence of platinum wire as AE (axillary electrode) and Ag/AgCl (3 M KCl) as a RE (reference electrode) connected with *CS* as WE (working electrode). EMs for *CS* were performed after OCP (open circuit potential) time (30 min) in presence and absence of various concentrations of *Ar-Sb* inhibitor. EIS technique was performed at frequency range of 100 kHz - 0.1 Hz and 5 mV amplitude. Some kinetic parameters of the corrosion reaction such as solution resistance (R_s), polarization resistance (R_P) and constant phase element (*CPE*) were recorded. After EIS,

Table 1
EIS parameters for CS in 1.0 M HCl solution with and without different concentrations of Ar-Sb inhibitor at room temperature.

Inh.	Conc, M	R_s, ($\Omega.cm^2$)	R_P, ($\Omega.cm^2$)	*CPE*		C_{dl}, (F/cm^2) × 10^{-5}	R_L ($\Omega.cm^2$)	*L* (H)	*τ*, s	Θ	η
				Y_O, μsn Ω^{-1} cm^{-2}	N						
Blank	0.00	3.49	28.21	426.5	0.869	15.51	——	——	0.0013	——	——
Ar-Sb	5×10^{-6}	3.61	115.16	214.7	0.688	1.92	2.1	1.34	0.0022	0.7566	75.52
	1×10^{-5}	3.82	202.29	141.2	0.579	1.77	6.6	1.88	0.0036	0.8608	86.05
	5×10^{-5}	4.02	259.09	117.5	0.738	1.72	10.9	2.34	0.0045	0.8912	89.11
	1×10^{-4}	7.19	335.22	71.7	0.639	1.68	13.1	2.99	0.0056	0.9160	91.58
	5×10^{-4}	7.45	497.21	71.06	0.673	1.28	——	——	0.0064	0.9433	94.32

PDP was measured using scan rate 1 mV/s and potential range ± 300 mV around OCP. Corrosion current density (i_{corr}), corrosion potential (E_{corr}), both anodic and cathodic Tafel slopes (β_a and β_c), and corrosion rate (*r*) were extracted from Tafel slope and discussed. In addition, the thermodynamic parameters of *CS* in absence and presence of *Ar-Sb* were calculated and discussed using EMs at temperature range (20, 30, 45 and 60 °C). For more information about the stability of *Ar-Sb* film, CV measurements were also applied for *CS* in 1 M HCl electrolyte with and without 5×10^{-4} M of *Ar-Sb* inhibitor. The mean values of the repeated experiments were recorded. The uncertainty values for the polarization resistance (R_P) and those of corrosion current densities (i_{corr}) have been calculated and reported in Table 1Si.

2.4. Quantum study

Material studio software (Ms 6.0) was used to obtained FMO (Frontier molecular orbitals) of the studied *Ar-Sb* in both gas and liquid phases. Based on DFT, DMol3 module was used for GO (Geometry Optimization) of the studied *Ar-Sb* in both gas and liquid phases using GGA (Generalized Gradient Approximation) method with DNP-3.5 (Double Numerical plus polarization) basis set. The inhibition effect of the studied *Ar-Sb* was discussed using quantum chemical parameters such as HOMO (Highest Occupied Molecular Orbital) and LUMO (Lowest Unoccupied Molecular Orbital) which were calculated after the optimization of *Ar-Sb*. For more information about the ability of *Ar-Sb* to suppress *CS* corrosion, the interaction between *Ar-Sb* and Fe (110) was simulated based on MCs in both gas and liquid phases. The adsorption of *Ar-Sb* over Fe (110) was achieved using adsorption locator module by using the optimized structure of *Ar-Sb* and aggressive particle (200 H_2O + 20 H_3O^+ + 10 Cl^-) under COMPASS (Condensed phase Optimized Molecular Potentials for Atomistic Simulation Studies) force field-controlled [28].

2.5. Surface analysis

The surface morphology of *CS* sample (1 ×1 ×0.3 cm) was studied in 1 M HCl free and containing 5×10^{-4} M of *Ar-Sb* for more information about *CS* corrosion process and the inhibition power of *Ar-Sb* using SEM technique after 6 h at a magnification of 4000 X and an accelerating voltage of 20 keV (R) QUANTA FEG 250. Also, the inhibition performance of the studied *Ar-Sb* in 1 M HCl was confirmed using EDX unit attached to SEM by detection the elemental analysis of the outer *CS* surface and AFM for 3D images of *CS* specimen in X, Y and Z coordination axis.

3. Results and discussion

3.1. Electrochemical measurements

3.1.1. Electrochemical impedance spectroscopic

It is imperative to achieve a steady state process before starting EMs in order to establish the original behavior of *CS*. E_{ocp} variation of *CS* with time in 1 M HCl free and containing different doses of *Ar-Sb* inhibitor until the steady-state potential was depicted as seen in Fig. 3Si. It was noticed that, OCP tends to be stable with time and less fluctuates were observed. Also, the rapidly and negligible variations in the OCP may be attributed to the modification of the interface surface at *Ar-Sb* concentrations with a steady-state had been achieved after 7 min. This result suggested that, *Ar-Sb* has more thermodynamically stable state and effective adsorption over *CS* surface[29]. Also, the addition of *Ar-Sb* inhibitor shifted E_{ocp} value to negative (cathodic) direction which can be explained by *Ar-Sb* adsorption over *CS* surface and dominate the cathodic reaction more than anodic reaction[8,30]. EIS is a highly sensitive method used for determination the electrical response of electrochemical system such as corrosion without any destruction[31].

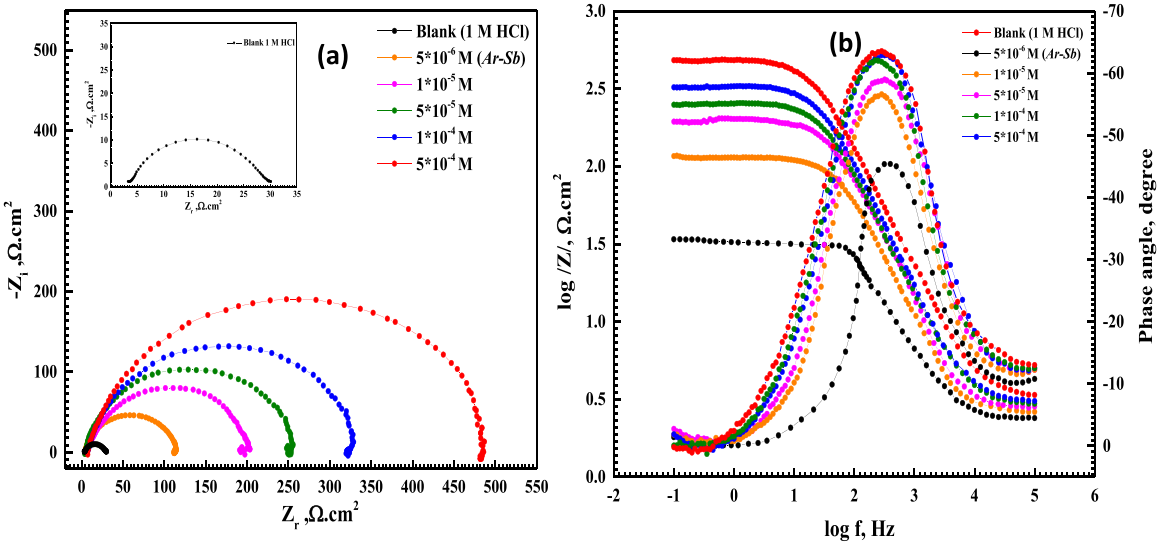

Fig. 1. Nyquist (a) and Bode-Phase (b) diagrams of *CS* in 1 M HCl in absence and presence of different concentrations of *Ar-Sb* inhibitor at room temperature.

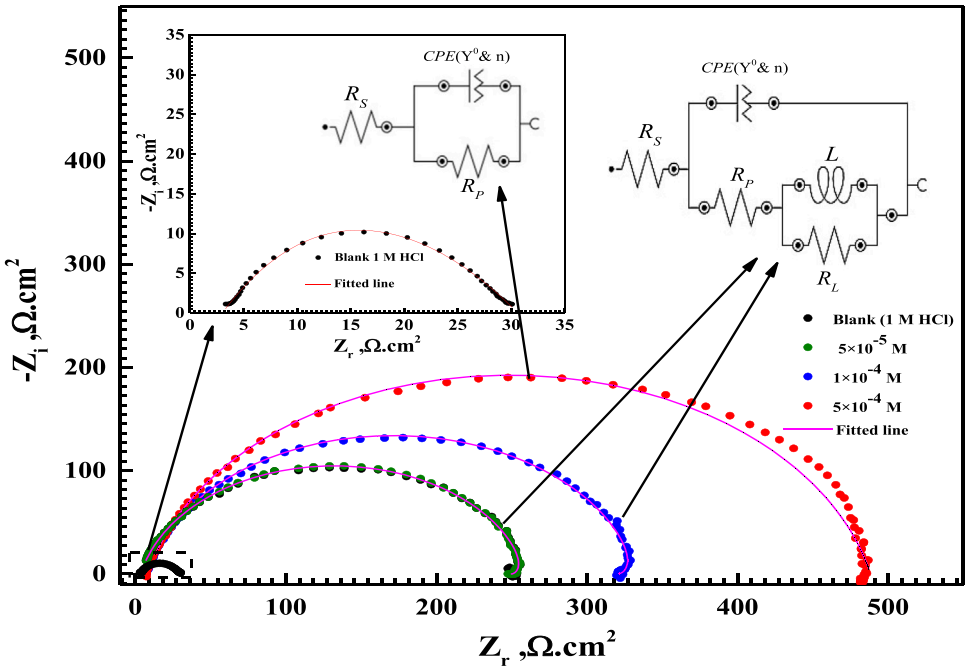

Fig. 2. Nyquist plots of *CS* in 1 M HCl in absence and presence of various concentrations of *Ar-Sb* inhibitor using the proposed equivalent circuit.

From EIS technique, the kinetics occurring at the steel solution interface could further be elaborated in depth via a non-destructive and a quasi-steady state approach[23]. At room temperature (20 °C), the corrosion process of *CS*/HCl interface was studied using non-destructive EIS technique based on AC (alternative current). The Nyquist and Bode-Phase diagrams of *CS* in 1 M HCl and various concentrations of the prepared *Ar-Sb* were presented as in Fig. 1. It was noticed that from Fig. 1, Nyquist curves were imperfect semicircle, and the linear slope of bode plots deviated from - 1. Also, at the intermediate frequency region, the maximum phase angle value in the absence and presence of *Ar-Sb* deviated from − 90. These observations were returned into the frequency dispersion phenomena which can be attributed to *CS* roughness and inhomogeneity besides the difference in diameters between electrons and *Ar-Sb* molecules, as electrons control charge on the metal side of the *CS*/solution interface, while *Ar-Sb* adsorbed molecules control charge on the solution side[31,32]. Nyquist curves of *CS* in Fig. 1 include depressed capacitive semicircle in absence and presence of *Ar-Sb*. This indicates the corrosion reaction mechanism of *CS* was controlled by Charge transfer process and doesn't change with the addition of *Ar-Sb* [33]. The diameter of Nyquist curves increases with rising *Ar-Sb* amounts which can be explained by enhancement in charge transfer resistivity during the introduction of *Ar-Sb* inhibitor compared to 1 M HCl free solution, thus indicating a better protection of *CS* surface against acid attack, consequently, suppress the rate of *CS* dissolution [34]. As seen in Fig. 1, the gap between bode curves of *Ar-Sb* and the uninhibited solution increases with rising of concentration. This demonstrates protection of *CS* against the aggressive HCl solution by formation of a protective film barrier of the adsorbed *Ar-Sb* molecules over *CS* surface[35]. At intermediate frequency, the value of the maximum phase angle increases with rising of *Ar-Sb* concentration to more negative value (−90°). Also, at low frequency region, the shift of modulus impedance /z/ to higher values can be explained by the adsorption of *Ar-Sb* molecules over *CS* surface [36].

Fig. 2 shows two various electrical equivalent circuit diagrams (EECDs) were used to define *CS*/solution interface. Where, Nyquist plots of *CS* in 1 M HCl free and 5 × 10^{-4} M of *Ar-Sb* can be fitted with a simple Randles equivalent circuit consists of one capacitive loop which can be related to R_s (solution resistance), R_P (polarization resistance), and *CPE* (constant phase element) which can be clarified with Y_o and coefficient n[37,38]. While Nyquist plots of *CS* in presence of higher concentrations of *Ar-Sb* inhibitor consist of a depressed capacitive half-circle at high and middle frequency regions following with a second inductive loop appeared at low frequencies which indicates the inability of the soluble corrosion products to adhere strongly to *CS* surface and to separate[31, 39]. The appearance of inductive loop at low-frequency can be attributed to the relaxation of the adsorbed *Ar-Sb* molecules or metal–organic complexes and redissolution processes as well as unstable species at *CS*/solution interface[22,40]. Therefore, the capacitive loop of *Ar-Sb* inhibitor is related to R_p which contains R_{ct}, R_d (diffuse layer resistance), R_f (film resistance) and R_a (accumulations at metal/solution resistance) which provides a barrier effect[31]. These observations suggested EECD as in Fig. 2 consists of R_s, CPE, R_p, L (inductance), and R_L (inductive loop resistance). Also, the disappearance of inductive loop in presence of high concentration (5 ×10^{-4} M) indicates that a stable and tighter films formation of *Ar-Sb* molecules over *CS* surface[23,40]. The kinetic parameters of the corrosion reaction used to evaluate the corrosion behavior of *CS* in absence and presence of *Ar-Sb* inhibitor using the proposed electrical equivalent circuit diagram (EECD) were extracted and listed in Table 1. As seen in Table 1, the addition of *Ar-Sb* inhibitor shifted the value of coefficient n to lower value which can be explained by irregular current distribution arises from roughness and defects of surface indicating *CS* surface become more homogeneous due to the adsorption of *Ar-Sb* molecules or metal–organic complexes [34,41]. Also, the n value < 1 (between 0.579–0.869) is due to *CS*/solution interface not behaving as an ideal capacitor[39,42]. Also, Y_o value decreases with the addition of *Ar-Sb* inhibitor which can be attributed to increase thickness (*T*) of the adsorbed layer on *CS* surface by replacement of corrosive particles with *Ar-Sb* molecules[28,43]. The C_{dl} (double layer capacitance) replaced by *CPE* giving a more accurate and favorable *EIS* results[44].*CPE* impedance (Z_{CPE}) was determined using the following equation:

$$Z_{CPE} = Q^{-1}(i\omega_{max})^{-n} \quad (1)$$

$$C_{dl} = \left(\frac{\varepsilon^{\circ}\varepsilon}{T}\right)A \quad (2)$$

where, *Q*, ω_{max} *A*, , ε∘ and ε are constant phase element, angular frequency, electrode surface area, the permittivity of air and the local

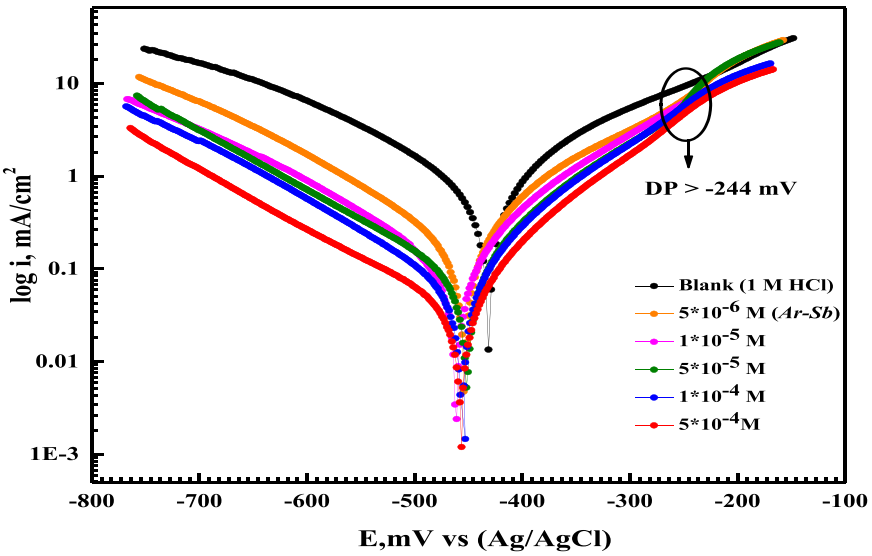

Fig. 3. PDP curves of *CS* in 1 M HCl in absence and presence of various concentrations of *Ar-Sb* inhibitor at room temperature.

dielectric constant[45,46]. The values of C_{dl} and τ (relaxation time) can be calculated according to the following equations:

$$C_{dl} = 1/(2\pi R_P F_{img\rightarrow Max}) \quad (3)$$

$$\tau = C_{dl} \times R_P \quad (4)$$

where, $F_{img\rightarrow Max}$ is the frequency at maximum imaginary impedance [47]. As in Table 1, C_{dl} value decreases as *Ar-Sb* concentration increases. This behavior can be explained by shielding of *CS* surface from the corrosive electrolyte by formation of a protective layer of *Ar-Sb* molecules consequently decrease the direct contact between *CS* surface and the aggressive HCl through the adsorption process of *Ar-Sb* via its active centers such as: hetero atoms (nitrogen atoms), and π-electrons (C═N and benzene ring) [48]. The addition of *Ar-Sb* inhibitor shifts τ value to high values till reaches 0.0022 s and 0.0064 s for 5×10^{-6} M and 5×10^{-4} M respectively, compared to the blank solution (1 M HCl) 0.0013 s. This reveals that *Ar-Sb* molecules are adsorbed slowly on *CS* surface subsequently, the adsorption time process becomes much higher with formation of stable film layer of *Ar-Sb* molecules shielded *CS* surface[28,49].

The addition of *Ar-Sb* inhibitor to the corrosive media offers high protection to *CS.* surface. This behavior can be observed in the value of θ (surface coverage) and η (inhibition efficiency) in Table 1. The values of θ and η were calculated based on R_P values and according to equations:

$$\theta = (R_{P.Ar-Sb} - R_{P.blank})/R_{P.inh}) \quad (5)$$

$$\eta = \theta \times 100 \quad (6)$$

Where, $R_{P.Ar-Sb}$ and $R_{P.blank}$ are the charge transfer resistance of *Ar-Sb* and blank solution respectively[50]. R_P value increase with the addition of *Ar-Sb* inhibitor till reach 115.87 Ω.cm^2 and 497.38 Ω.cm^2 in presence of 5×10^{-6} M and 5×10^{-4} M respectively relative to blank solution (1 M HCl) 28.23 Ω.cm^2. This can be attributed to the adsorption of *Ar-Sb* molecules over *CS* surface increases with concentration by replacing more corrosive molecules (H_2O and Cl^-) and blocking more uncover sites of *CS* surface indicating that the thickness of *Ar-Sb*-adsorption film increases as concentration increases[51]. Also, a decline in the electrolyte conductivity was observed with the addition of *Ar-Sb* inhibitor owing to the adsorption of *Ar-Sb* molecules over *CS*. This behavior can be noticed in R_S values as in Table 1 which denotes that, *CS* surface is shielded by the adsorbed *Ar-Sb* molecules and the surface coverage of *CS* increases with addition *Ar-Sb* molecules[34,52]. The inhibition potency of *Ar-Sb* inhibitor increases as concentration increases till touch 75.66% and 94.33% in presence of 5×10^{-6} M and 5×10^{-4} M respectively, which exhibited that, *Ar-Sb* act as an efficient inhibitor for *CS* in aggressive 1 M HCl.

3.1.2. *Potentiodynamic polarization measurements*

The anti-corrosion behavior of *Ar-Sb* for *CS* in aggressive HCl was studied using PDP for more information about the anodic and cathodic reactions as shown in Fig. 3. From polarization curves in Fig. 3, the addition of *Ar-Sb* shifts both the anodic and cathodic Tafel lines to lower values (noble direction). This observation can be attributed to the high adsorption capacity of *Ar-Sb* to cover *CS* surface by blocking its active sites (uncover) and subsequently decrease the dissolution rate of *CS*[53]. The gap between semi logarithmic current - potential curves (log i - E) of *Ar-Sb* inhibitor and that of blank solution increases with rising of concentration due to the adsorption process of *Ar-Sb,* indicating that the existence of *Ar-Sb* inhibits *CS* corrosion process [54,55]. From Fig. 3, the parallel lines of polarization curves at cathodic region indicates the mitigation power of *Ar-Sb* inhibitor for *CS* corrosion in aggressive environment by blocking the active sites of *CS*. The blocking effect of *Ar-Sb* inhibitor cause a decline in H_2 evolution rate by decreasing the

Table 2
PDP parameters for *CS* in 1.0 M HCl solution with and without different concentrations of *Ar-Sb* inhibitor at room temperature.

Inh.	Conc, M	E_{corr}, (mV) Vs. Ag/AgCl	β_a (mV/dec)	β_c (mV/dec)	i_{corr} (mA/cm^2)	*r* (mm/year)	R_p (Ω.cm^2)	θ	**η**
Blank	0.00	-449.2	115.6	153.46	0.867	10.07	33.03	——	——
	5×10^{-6}	-453.8	103.8	150.8	0.184	2.149	127.43	0.788	78.81
	1×10^{-5}	-461.5	98.3	148.1	0.105	1.229	216.53	0.8788	87.88
Ar-Sb	5×10^{-5}	-469.4	89.7	151.2	0.086	1.001	262.32	0.9007	90.07
	1×10^{-4}	-456.2	83.2	147.6	0.061	0.709	319.47	0.9301	93.01
	5×10^{-4}	-457.4	78.1	166.2	0.036	0.426	502.76	0.9579	95.79

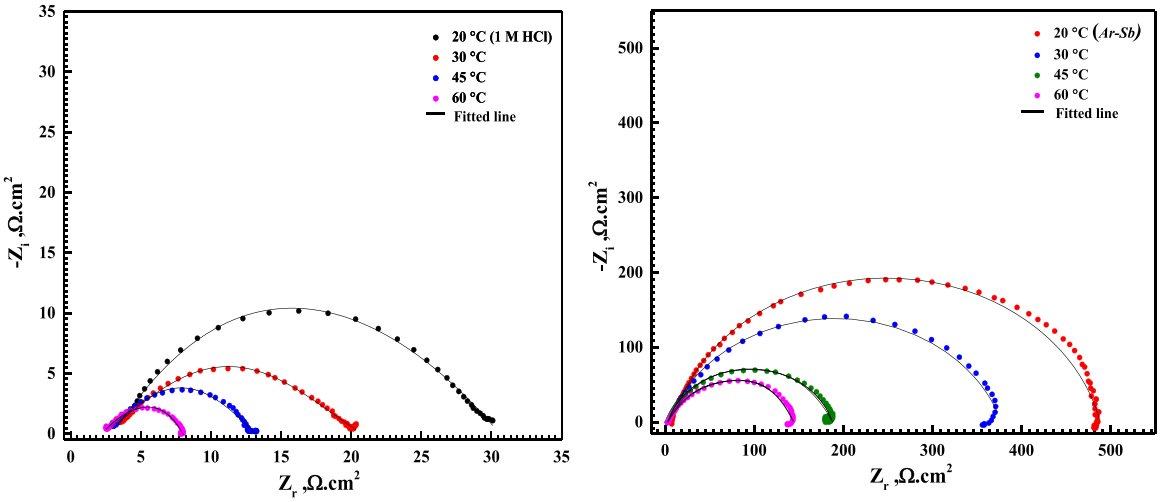

Fig. 4. Nyquist curves for *CS* in 1 M HCl in absence and presence of 5×10^{-4} M of *Ar-Sb* inhibitor at different temperature.

available surface area for H^+ by shielding *CS* surface with *Ar-Sb* layer. So, H_2 reduction is activated control and no modification in *CS* reaction mechanism [45]. At anodic region, the anodic Tafel lines give indication about the protection power of *Ar-Sb* inhibitor to protect *CS* against aggressive surrounding. Where, at low anodic potential, the corrosion performance of *Ar-Sb* inhibitor depends on the adsorption rate by forming a protective layer of adsorbed *Ar-Sb*[49]. While at anodic potential > −244 mV, the desorption rate of *Ar-Sb* molecules is higher than their adsorption rate which called desorption potential (DP) in which the dissolution rate and the current density of *CS* increase [56].

Table 2 shows the electrochemical kinetic parameters obtained from PDP curves based on Tafel extrapolation. θ and η values in Table 2 were calculated based on i_{corr} value as the following equation:

$$\theta = (i_{corr.blank} - i_{corr.inh})/i_{corr.blank} \quad (7)$$

$$\eta = \theta \times 100 \quad (8)$$

Data in Table 2, reveals the mitigation power of *Ar-Sb* for *CS* in aggressive HCl solution. The addition of *Ar-Sb* shifts i_{corr} value to lower values till reach 0.184 $mAcm^{-2}$ and 0.036 $mAcm^{-2}$ at 5×10^{-6} M and 5×10^{-4} M of the prepared *Ar-Sb* respectively, compared to 1 M HCl solution 0.867 $mAcm^{-2}$. It was noticed that, i_{corr} value decreases with rising of concentration consequently enhance the inhibition efficiency of *Ar-Sb* inhibitor due to its adsorption at *CS*/HCl interface [57]. This behavior reveals that, the adsorption of *Ar-Sb* over *CS* surface and decrease the corrosion process by decreasing the contact between the corrosive particles and *CS* surface by formation of a protective layer of adsorbed *Ar-Sb* molecules [15]. After the addition of *Ar-Sb* inhibitor, both anodic and cathodic Tafel slopes were slightly impacted with no notable change in β_a and β_c values as in Table 2, indicating no modification in *CS* corrosion reaction mechanism [58]. The addition of *Ar-Sb* shifted E_{corr} slightly to more -ve direction which reveals that a greater number of *Ar-Sb* molecules were adsorbed on *CS*/HCl interface and consequently, suppress the cathodic corrosion reaction more than anodic reaction[5,59]. Also, the variation in E_{corr} value of the treated solutions was with ± 85 mV range compared with the untreated one, signifying that *Ar-Sb* inhibitor acted as mixed-type inhibitor (anodic and cathodic) for *CS* in 1 M HCl solution by blocking both anodic and cathodic sites on *CS* surface through the adsorption process via its active centers such as hetero atoms (N) and π-electrons (C═N and benzene ring) [60]. The tabulated η value in Table 2 increases as the concentration increases which can be explained by increase in number of the adsorbed *Ar-Sb* molecules over *CS* surface consequently surface coverage of active sites increases which offers high protection of *CS* against corrosive 1 M HCl solution [61]. The inhibition power of *Ar-Sb* increases till touch 78.81% and 95.79% at 5×10^{-6} M and 5×10^{-4} M of *Ar-Sb* respectively, indicating that *Ar-Sb* inhibits *CS* corrosion process effectively in 1 M HCl solution. The obtained from both PDP and EIS techniques were closed and in a good agreement with each other which increases the trust in the experimental data. The as-obtained inhibition efficiency for the studied *Ar-Sb* inhibitor was much higher than many previously reported inhibitors in the same electrolyte (1 M HCl) as in Table 2Si.

Table 3
EIS parameters for CS in 1.0 M HCl free and containing 5×10^{-4} M of Ar-Sb inhibitor at different temperature.

Inh.	**Temp.** °C	R_s, (Ω.cm²)	R_P, (Ω.cm²)	*Θ*	η
Blank	20	3.49	28.2	—	—
	30	3.14	16.84	—	—
	45	2.87	10.01	—	—
	60	2.58	5.50	—	—
Ar-Sb	20	7.45	497.38	0.9433	94.33
	30	3.83	383.57	0.956	95.61
	45	2.62	192.81	0.9481	94.81
	60	5.31	144.12	0.9618	96.18

3.2. *Film stability and adsorption at harsh conditions*

The protective film stability of the adsorbed *Ar-Sb* molecules over *CS* surface in 1 M HCl at 5×10^{-4} M was investigated at harsh conditions such as different temperature and immersion times using EIS technique. Also, *Ar-Sb* film stability on *CS* surface was tested via CV technique.

- ***Effect of Temperature***

  The mitigation performance of *Ar-Sb* inhibitor in 1 M HCl solution for *CS* was studied at temperature range (20, 30, 45 and 60 °C). The kinetic energy of the system increases with temperature rising consequently, increases the kinetic motion of corrosive media. This behavior decreases both corrosion products deposited and even the adsorbed *Ar-Sb* film covering *CS* surface which makes the exposed *CS* surface area subjected to destructive solution increases and finally increases iron ionization and H_2 evolution[25]. Nyquist spectra of *CS* in 1 M HCl free and after addition 5×10^{-4} M of *Ar-Sb* appeared with a semicircular shape decreased in diameter with temperature rising as seen in Fig. 4, indicating that *CS* corrosion reaction mechanism not affected by temperature[62]. The values of η in Table 3 increased slightly with rising of temperature till reach 96.18% at 60 °C. This reflected the inhibition power of *Ar-Sb* over the temperature range and its adsorption on *CS* surface as a stable film layer against the

Table 4
EIS parameters for CS in 1.0 M HCl free and containing 5×10^{-4} M of Ar-Sb inhibitor at different immersion time.

Inh.	t, h	R_s, ($\Omega.cm^2$)	R_P ($\Omega.cm^2$)	Θ	η
Blank	0.5 h	3.49	28.23	—	—
	1 h	3.28	22.35	—	—
	2 h	3.14	18.44	—	—
	4 h	3.03	15.65	—	—
	6 h	3.05	12.90	—	—
Ar-Sb	0.5 h	7.45	497.38	0.9432	94.32
	1 h	5.48	471.82	0.9526	95.26
	2 h	8.43	439.17	0.9580	95.80
	4 h	4.43	425.96	0.9632	96.32
	6 h	1.70	392.74	0.9671	96.71

destructive action of HCl solution by formation of a chemical bonds between *Ar-Sb* active centers and vacant 3d-orbital of Fe (chemical adsorption)[63], [64].

- ***Effect of immersion time***

The *CS* surface was exposed to 1 M HCl solution with and without containing 5×10^{-4} M of *Ar-Sb* for different immersion time. The η (mitigation efficiency) values over various immersion time were presented in Table 4. The η values increased as immersion time increased till touch 96.71% after 6 h of immersion. This observation indicated the stability of *Ar-Sb* adsorbed layer over *CS* surface due to *Ar-Sb* molecules accumulation which decreased the destructive action of HCl [13]. Nyquist plot of *CS* in absence and presence of 5×10^{-4} M of *Ar-Sb* for long exposure time was presented as seen in Fig. 5 indicated that, the reaction mechanism of *CS* corrosion was not affected by immersion time [65]. In the presence of *Ar-Sb*, all R_P values were significantly high compared with those in acidic HCl free indicating that, the adsorbed *Ar-Sb* film protects *CS* surface from the aggressive action of acidic HCl solutions[49]. R_P values of *CS* in 1 M HCl in Table 4 decrease with time (from 28.23 $\Omega.cm^2$ to 12.9 $\Omega.cm^2$). This reflected that *CS* surface was more susceptible to corrosive particles (corrosion process), therefore the dissolution rate increased with time [66]. Also, R_P value in presence of *Ar-Sb* dropped slightly with time which can be explained by some defects in *Ar-Sb* film layer caused by the aggressive HCl which evolved H_2 gas. From Table 4, R_P value at 5×10^{-4} M of *Ar-Sb* was high compared to that of blank solution which confirming the mitigation power of *Ar-Sb* against corrosive surroundings at different immersion time [14].

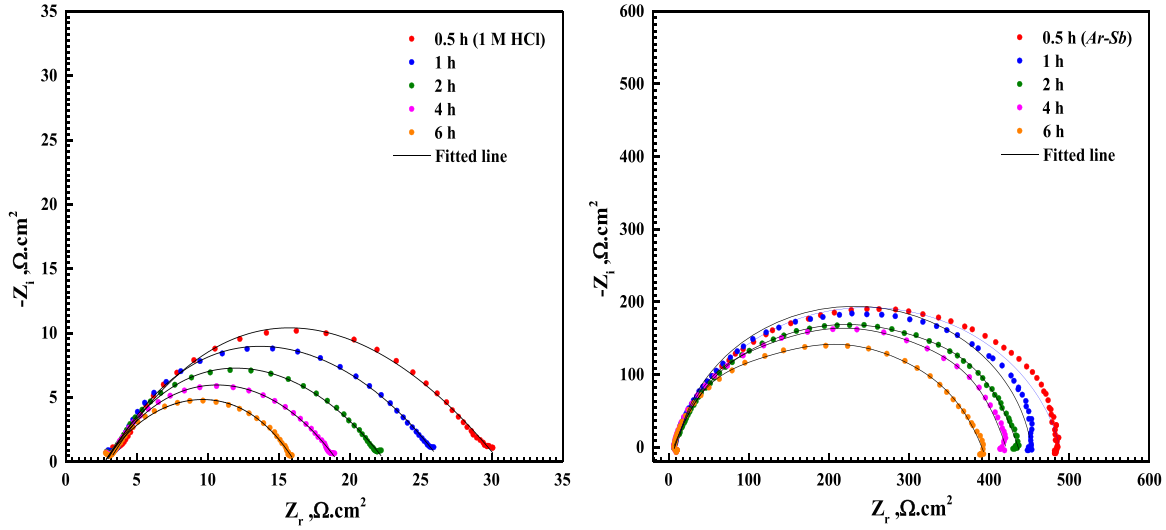

Fig. 5. Nyquist curves for *CS* in 1 M HCl in absence and presence of 5×10^{-4} M of *Ar-Sb* inhibitor after different immersion time.

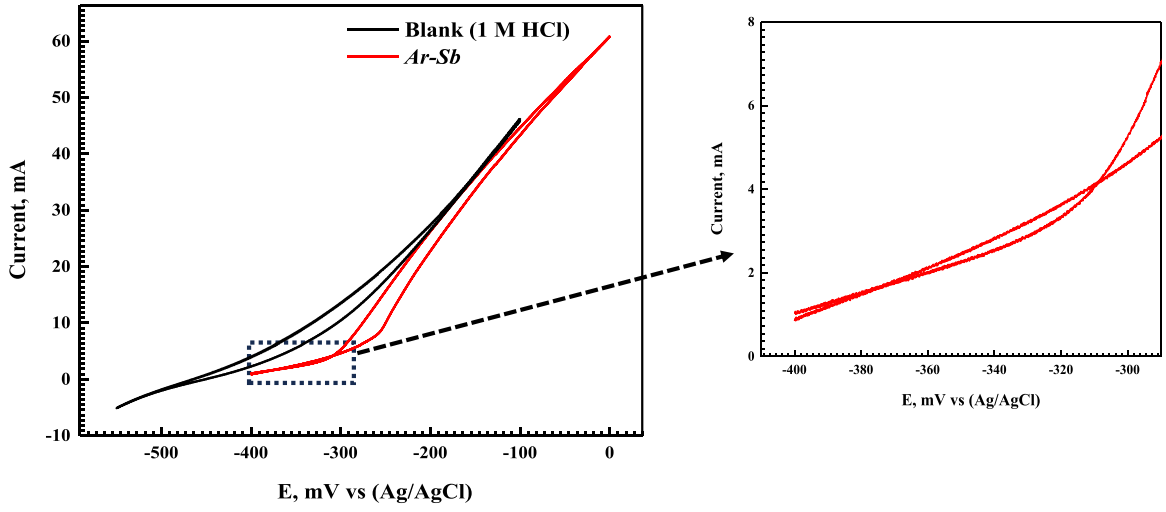

Fig. 6. Cyclic Voltammetric curves for *CS* in 1 M HCl free and containing 5×10^{-4} M of *Ar-Sb* inhibitor at scan rate10 mVs^{-1}.

Table 5
PDP parameters for CS in 1.0 M HCl free and containing 5 * 10–4 M of *Ar-Sb* inhibitor at different temperature.

Inh.	Temp. °C	E_{corr}, (mV) Vs. Ag/AgCl	i_{corr} (mA/cm^2)	β_a (mV/dec)	β_c (mV/dec)	*r* (mm/year)	R_P (Ω.cm^2)	*Θ*	*IE%*
Blank	20	-449.2	0.867	115.6	153.4	10.07	33.03	—	—
	30	-427.5	1.703	120.5	155.6	19.79	17.32	—	—
	45	-427.4	2.485	118.6	151.6	28.88	11.63	—	—
	60	-412.5	4.647	122.5	149.7	54.01	6.31	—	—
Ar-Sb	20	-457.4	0.036	78.1	166.2	0.426	502.8	0.9579	95.79
	30	-488.6	0.071	124.2	154.6	0.872	319.5	0.9586	95.86
	45	-503.2	0.122	125.1	141.5	1.549	173.6	0.9507	95.07
	60	-506.3	0.184	129.2	143.8	2.267	130.9	0.9604	96.04

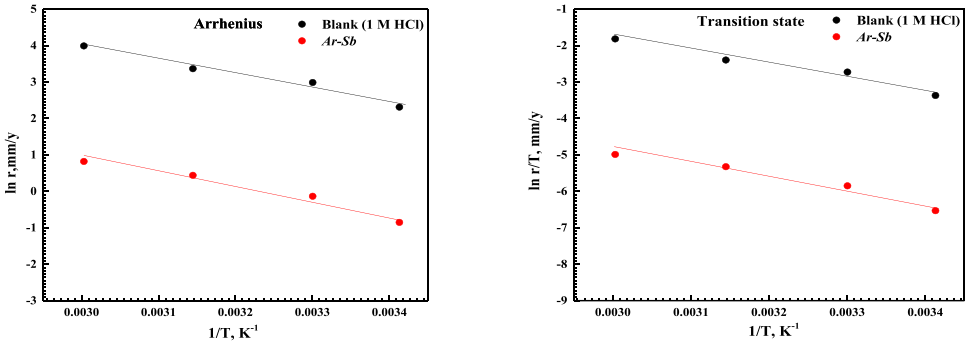

Fig. 7. Arrhenius and transition state relations against 1/T, for *CS* in 1 M HCl free and containing 5 × 10^{-4} M of *Ar-Sb*.

- ***Cyclic voltammetry***

Ar-Sb film stability over *CS* surface was also tested using Cyclic voltammetry technique in 1 M HCl free and containing 5 × 10^{-4} M of *Ar-Sb* inhibitor at scan rate 10 mVs^{-1} from − 550 mV (starting potential) to positive direction and reverse back to the starting potential as seen in Fig. 6. A notable shift was observed in the staring potential after the addition of *Ar-Sb* inhibitor (from −400 mV) relative to 1 M HCl free (from −550 mV) which can be attributed to *Ar-Sb* adsorption on *CS* surface. Also, a notable shoulder at − 256 mV was observed confirmed the adsorption of *Ar-Sb* inhibitor on *CS* surface via hetero atoms (N-atoms) in its structure[67]. These observations reflected the blocking effect of *Ar-Sb* inhibitor and formation of a protective layer of *Ar-Sb* molecules over *CS* surface. The appearance of hysteresis shape from − 400 mV to − 300 mV as in Fig. 6 indicated a such complexing processes lead to a further decrease in the free Fe ions at the *CS* surface due to a bi-layer formation of *Ar-Sb* molecules via electrostatic attraction between the charged centers in *Ar-Sb* structure and Cl^- ions adsorbed on *CS* surface[68]. All these observations reflected the existence of *Ar-Sb* inhibitor and its mitigation role in *CS* dissolution[69].

3.3. Activation thermodynamic parameter

The Inhibition performance of *Ar-Sb* inhibitor was also investigated at different temperatures via PDP technique using the highest concentration (5 ×10^{-4} M) as in Fig. 4Si. Data extracted from Fig. 4Si were listed in Table 5 showed that, as the temperature increases, the values of *r* and i_{corr} of *CS* increase. In the presence of *Ar-Sb*, *r* and i_{corr} value were significantly low compared with those in free HCl solution reflected the adsorption of *Ar-Sb* molecules over *CS* surface and formation of a barrier layer against the aggressive action of HCl solutions[49]. η value in Table 5 increases slightly with temperature rising till touch 95.79% at 20 °C and 96.04% at 60 °C. This exhibited the temperature variation had no significant effect on *Ar-Sb* inhibition efficiency or its mitigation power which reflected the chemical adsorption of *Ar-Sb* on *CS* surface [46,70].

The corrosion kinetics of *CS* in the uninhibited and inhibited solutions was obtained using Arrhenius and Transition state equations:

$$\text{Arrhenius}: \quad \ln r = \ln A - \left(\frac{E_a}{RT}\right) \tag{9}$$

$$\text{Transition state}: \ln(r/T) = \left[\ln\left(\frac{R}{N_A h}\right) + \left(\frac{\Delta S^*}{R}\right)\right] - \left(\Delta H^* \Big/ RT\right) \tag{10}$$

Where, A, E_a, ΔH* , ΔS* , T and R are Arrhenius constant, activation energy, activation enthalpy, activation entropy, T is the absolute temperature, and R is the gas constant. N_A and *h* are Avogadro's number and Plank constant[46]. The value of E_a was calculated from the slope of linear relationship of (Ln *r* vs. 1/T) as in Fig. 7 with R^2 (linear regression coefficients) was very close to 1 as in Table 6. This indicated that, the corrosion of *CS* in absence and presence of *Ar-Sb* followed Arrhenius equation[71]. From Table 6, no notable change in the computed E_a values indicated that *Ar-Sb* was adsorbed on *CS* surface chemically. Also, E_a value was 32.208 kJ.mol^{-1} and 33.206 kJ.mol^{-1} in 1 M HCl and *Ar-Sb* respectively. This may be attributed to the competitive adsorption of *Ar-Sb* with water molecules on *CS* surface whose its desorption from surface required also some activation energy and may be linked with the

Table 6
Activation thermodynamic parameters for CS in the absence and presence of Ar-Sb inhibitor at different temperatures.

Inh.	Arrhenius			Transition state			
	slope	R^2	E_a (kJ mol^{-1})	*slope*	*intercept*	ΔH* (kJ mol^{-1})	ΔS* (J mol^{-1})
Blank	-3873.99	0.9757	32.21	-3561.8	8.878	29.61	-123.75
Ar-Sb	-3993.99	0.9671	33.21	-3681.8	6.163	30.62	-146.28

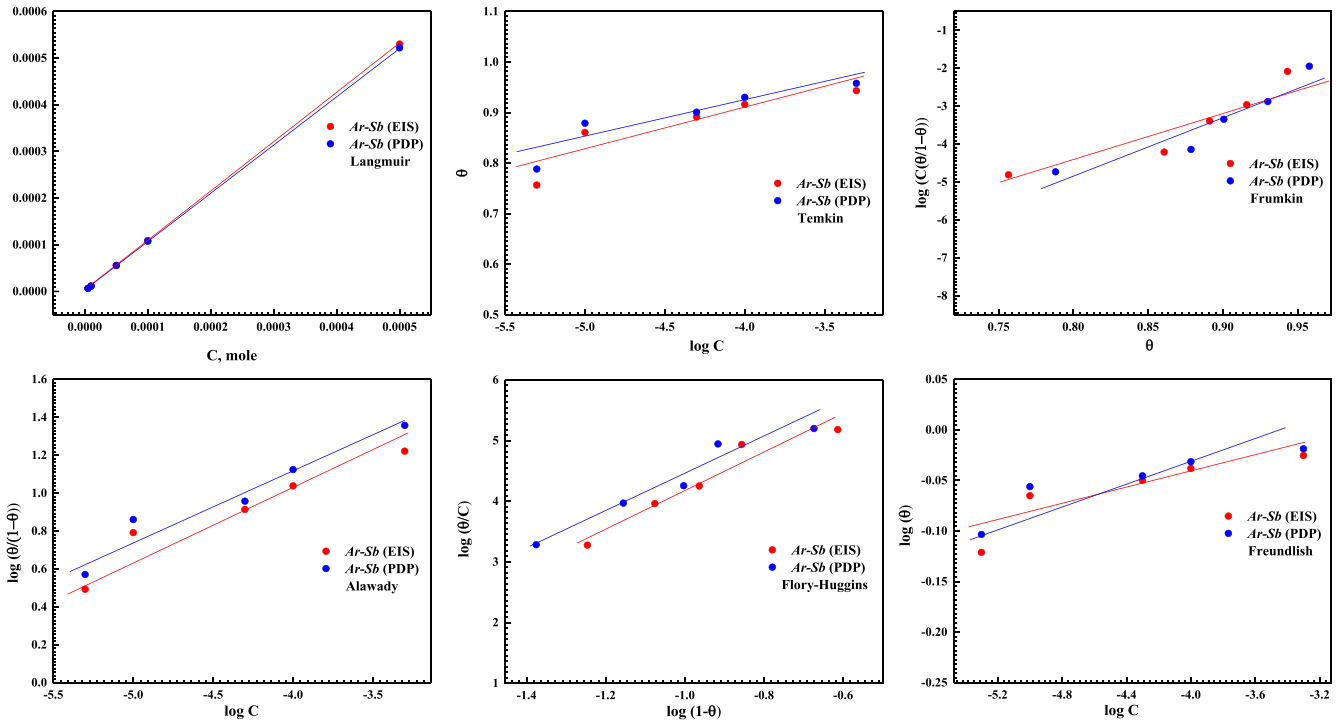

Fig. 8. various isotherms of *Ar-Sb* adsorption at *CS*/HCl interface using EIS and PDP data at room temperature.

Table 7
Various isotherms parameters of Ar-Sb adsorption at CS/HCl interface using EIS and PDP data at room temperature.

Isotherm	EIS					PDP				
	Slope	*intercept*	R^2	K_{ads} L.mol^{-1}	ΔG^{o}_{ads} kJ.mol^{-1}	*Slope*	*intercept*	R^2	K_{ads} L.mol^{-1}	ΔG^{o}_{ads} kJ.mol^{-1}
Langmuir	1.056	2.21×10^{-6}	1	45.2×10^{4}	-41.51	1.041	2.18×10^{-6}	0.9999	4.6×10^{5}	-41.53
ALawady	0.331	2.340	0.9297	11.9×10^{5}	-49.47	0.358	2.541	0.9439	1.3×10^{7}	-49.63
Flory-Huggins	3.111	7.279	0.9333	19.1×10^{5}	-50.62	2.845	7.246	0.9333	1.7×10^{7}	-50.43
Temkin	0.081	1.232	0.8189	1.14×10^{15}	-94.25	0.074	1.218	0.8431	2.1×10^{16}	-101.32
Frumkin	13.733	-15.487	0.8664	1.9×10^{-7}	27.93	15.70	-17.40	0.8891	2.8×10^{-8}	32.60
Freundlish	0.042	0.122	0.7951	1.325	-10.47	0.037	0.111	0.8231	1.291	-10.41

rise of C_{dl} thickness that increase the activation energy of the corrosion process[44], [72]. The ΔH* value with +ve sign reflected the endothermic behavior of *CS* dissolution which reflected the difficulty of *CS* dissolution process after the addition of *Ar-Sb* [73,74]. The ΔS* value in Table 6 with -ve sign reflected that the activated complex association in the rate determining step was rather than dissociation implying that more order takes place (from reactant to activated complex) leading to rising of *Ar-Sb* inhibition efficiency[75], [76].

3.4. Adsorption isotherm

Various adsorption isotherms such as Flory, Frumkin, Temkin, Alawady, Freundlich and Langmuir isotherms as in Fig. 8 were performed based on the obtained θ values from EIS and PDP for more information about the corrosion inhibition mechanism of the studied of *Ar-Sb* and its interaction with *CS* surface which can explained by replacement of the adsorbed water molecules (nH_2O_{ads}) from *CS* surface by the adsorbed molecules of *Ar-Sb* (*Ar-Sb*$_{ads}$). According to the following equation:

$$Ar\text{-}Sb_{sol} + nH_2O_{ads} \leftrightarrow Ar\text{-}Sb_{ads} + nH_2O_{sol} \quad (11)$$

The data obtained from EMs was more fitted with Langmuir model based on correlation coefficient value (R^2 =1) and can be defined using the following equation:

$$C/\theta = \left(\frac{1}{K_{ads}}\right) + C \quad (12)$$

$$\Delta G^{\circ}_{ads} = -RT\ln(55.5K_{ads}) \quad (13)$$

Where, C and K_{ads} andΔG°_{ads} were *Ar-Sb* concentration (M), adsorption equilibrium constant and the Gibbs free energy respectively. 55.5 is water concentration.

(mole L^{-1}) [77]. The K_{ads} value tabulated in Table 7 reflected strong interaction between *Ar-Sb* and *CS* surface via electron sharing process (donor-acceptor) via

N atoms and benzene ring with the vacant 3d-orbital of Fe forming strong chemical bond consequently forming high stable film of the adsorbed *Ar-Sb* molecules [78], [79]. The calculated G°_{ads} in Table 7 was − 41.53 kJ/mol and − 41.50 kJ/mol using PDP and EIS techniques respectively, confirming that *Ar-Sb* adsorbed on *CS* surface chemically [80]. Also, the -ve sign of G°_{ads} revels that *Ar-Sb* adsorption was a spontaneous process and usually characteristic of powerful interaction and a highly efficient adsorption[81,82].

3.5. Quantum chemical study

3.5.1. Density functional theory

Theoretical study of the prepared *Ar-Sb* inhibitor was performed to

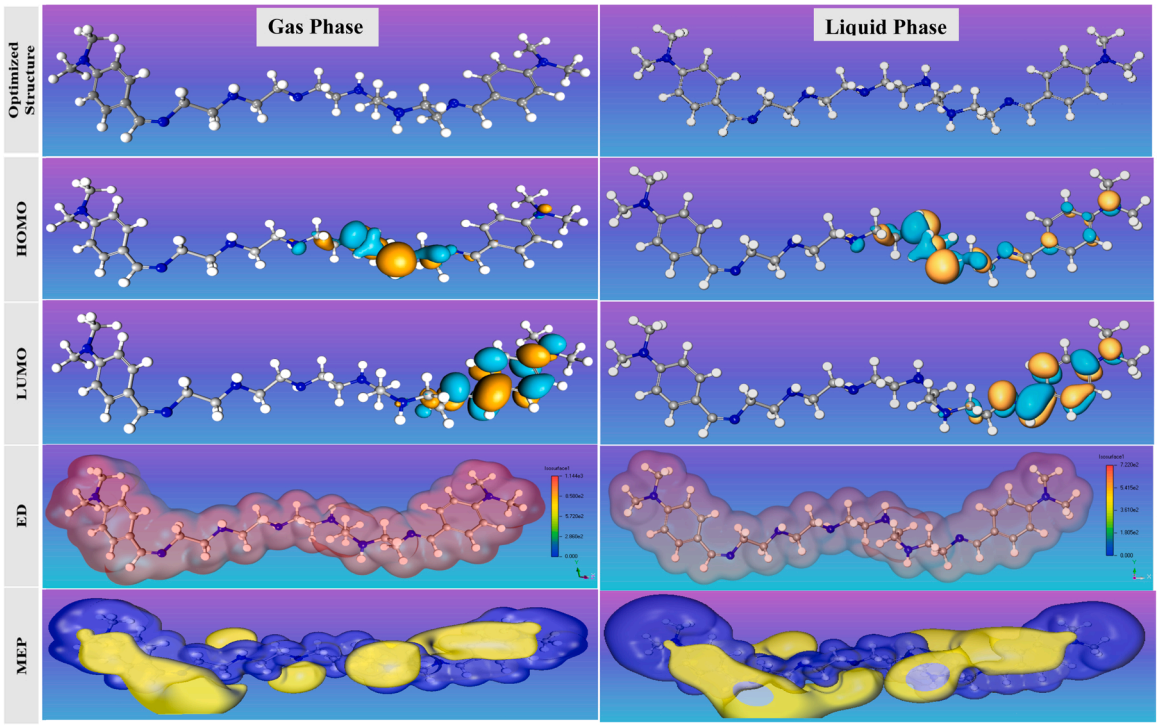

Fig. 9. Optimized structures, HOMO, LUMO, ED and MEP of the studied *Ar-Sb* in gas and liquid phases.

give more information about the relation between η and the molecular/electronic structure of *Ar-Sb* and its inhibition mechanism. The optimized structure of the investigated.

Ar-Sb and its FMOs (HOMO and LUMO) were represented as in Fig. 9. The optimized structure in Fig. 9 denotes the chemical structure of *Ar-Sb* which has the lowest energy with the most stable atoms arrangement [83–85]. The planarity of the optimized structure indicates that *Ar-Sb* has high probability of interacting with *CS* surface[25]. HOMO and LUMO distributions of *Ar-Sb* inhibitor in Fig. 9 suggested that HOMO represents the electron cloud of the nucleophile centers distributed on (N = C, NH, and N-CH_3) attached to benzene ring and ethylene spacer which reveals formation of a chemical bond (co-ordination bond) via electron donation transfer to the vacant d-orbital of Fe [28]. While LUMO represents the electron cloud of the electrophile centers distributed on (benzene ring, N = C, and N-CH_3) which reflected electron acceptance transfer from *CS* surface via back donation[61]. As noticed in HOMO and LUMO, the electron clouds are distributed over the whole structure of the studied *Ar-Sb* inhibitor which indicates the electron sharing between *Ar-Sb* inhibitor and *CS* surface via electron donation-acceptance transfer confirming the adsorption capability of *Ar-Sb* molecules over *CS* surface to form a protective dense layer[86]. Also, the electron density (ED) distribution over the studied inhibitor as in Fig. 9 reveals the adsorption capacity of *Ar-Sb* over *CS* surface and formation of a dense film layer of *Ar-Sb* molecules shielding the exposed *CS* surface[87,88]. Fig. 9 depicts the molecular electrostatic potential (MEP) isosurfaces of the studied *Ar-Sb* with its active sites (electron accumulation and electron loss) where *Ar-Sb* molecules interact with *CS* which are in agreement with HOMO and LUMO[28,89]. μ (dipole moment) is another index gives more information about the asymmetry of charge distribution through determination the size of the polarization deformation ability of *Ar-Sb* molecules and explains the electrostatic interactions between *Ar-Sb* molecules and *CS* surface[39,42,86]. The lower μ value, the lower mitigation potency. On the other hand, the other view proposes that, the higher μ values, the higher *Ar-Sb* interaction with *CS* surface and formation of dipole–dipole interaction consequently enhance the inhibition power[86], [90].

HOMO and LUMO energies (E_{HOMO} and E_{LUMO}) were used to calculate the relative quantum indices and listed in Table 8 as the following equations:

$$\Delta E_{gap} = E_{LUMO} - E_{HOMO} \tag{14}$$

$$\eta = \frac{\Delta E_{gap}}{2} \tag{15}$$

$$E_{b\to d} = \frac{-\eta}{4} \tag{16}$$

$$\chi = \frac{-(E_{HOMO} + E_{LUMO})}{2} \tag{17}$$

$$\Delta N = \frac{(\varphi_{Fe} - \chi_{inh.})}{2(\eta_{Fe} + \eta_{inh.})} \tag{18}$$

Where, ΔE_{gap}, η and $E_{b\to d}$ are the energy gap, global hardness and the energy of back donation. χ, ΔN and φ are the electronegativity, fraction of electron transfer and work function of Fe (1 1 0) plan = 4.82 eV [28, 91]. The values of E_{HOMO} and E_{LUMO} indicated the interaction between *Ar-Sb* inhibitor and *CS* surface via electron sharing through electron donation-acceptance process with 3-d orbital of Fe [3,91]. Furthermore,

Table 8
Computed Quantum chemical parameters of the studied Ar-Sb in gas and liquid phases.

Phase	E_{HOMO} (eV)	E_{LUMO} (eV)	ΔE_{gap} (eV)	η (eV. mol^{-1})	$E_{b\to d}$ (eV. mol^{-1})	χ (eV.mol^{-1})	ΔN	μ (Debay)
Gas Phase	-3.701	-1.027	2.674	1.337	-0.3342	2.364	0.9184	4.972
Liquid Phase	-4.281	-1.594	2.687	1.343	-0.3358	2.937	0.7006	7.196

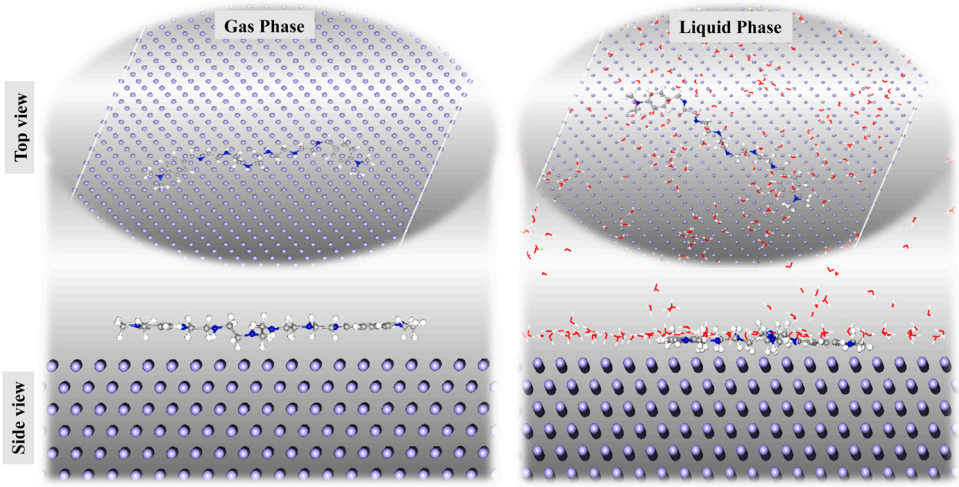

Fig. 10. Equilibrium adsorption configuration of the studied *Ar-Sb* in gas and liquid phases on the Fe (110) obtained by MCs simulations.

Table 9
The outputs energies calculated by Monte Carlo simulation for Ar-Sb in gas and simulated liquid phases on Fe (1 1 0).

Phase	E_T (kJ/mol)	E_{ads} (kJ/mol)	$E_{rig.}$ (kJ/mol)	$E_{def.}$ (kJ/mol)	(dE_{ads} /dNi) (kJ/mol)			
					Ar-Sb	H_2O	H_3O^+	Cl^-
Gas Phase	-302.982	-317.85	-302.95	-14.90	-317.85	———	———	———
Liquid Phase	-11535.69	-22332.56	-11782.97	-10549.59	-310.86	-19.47	-119.64	-125.72

ΔE_{gap} value used as a function of the reactivity and chemical stability of *Ar-Sb* inhibitor and explained the ease of the charge transfer process. The small value of ΔE_{gap} as in Table 8, exhibited the ease of electron polarizability consequently the higher adsorption capacity of *Ar-Sb* [33]. η is an index of molecular hardness and characteristic of resistance to deformation or electron clouds polarization. The small value of η reflected the high adsorption of *Ar-Sb* molecules over *CS* surface [28]. χ is used to evaluate the global reactivity of the studied *Ar-Sb* inhibitor. χ

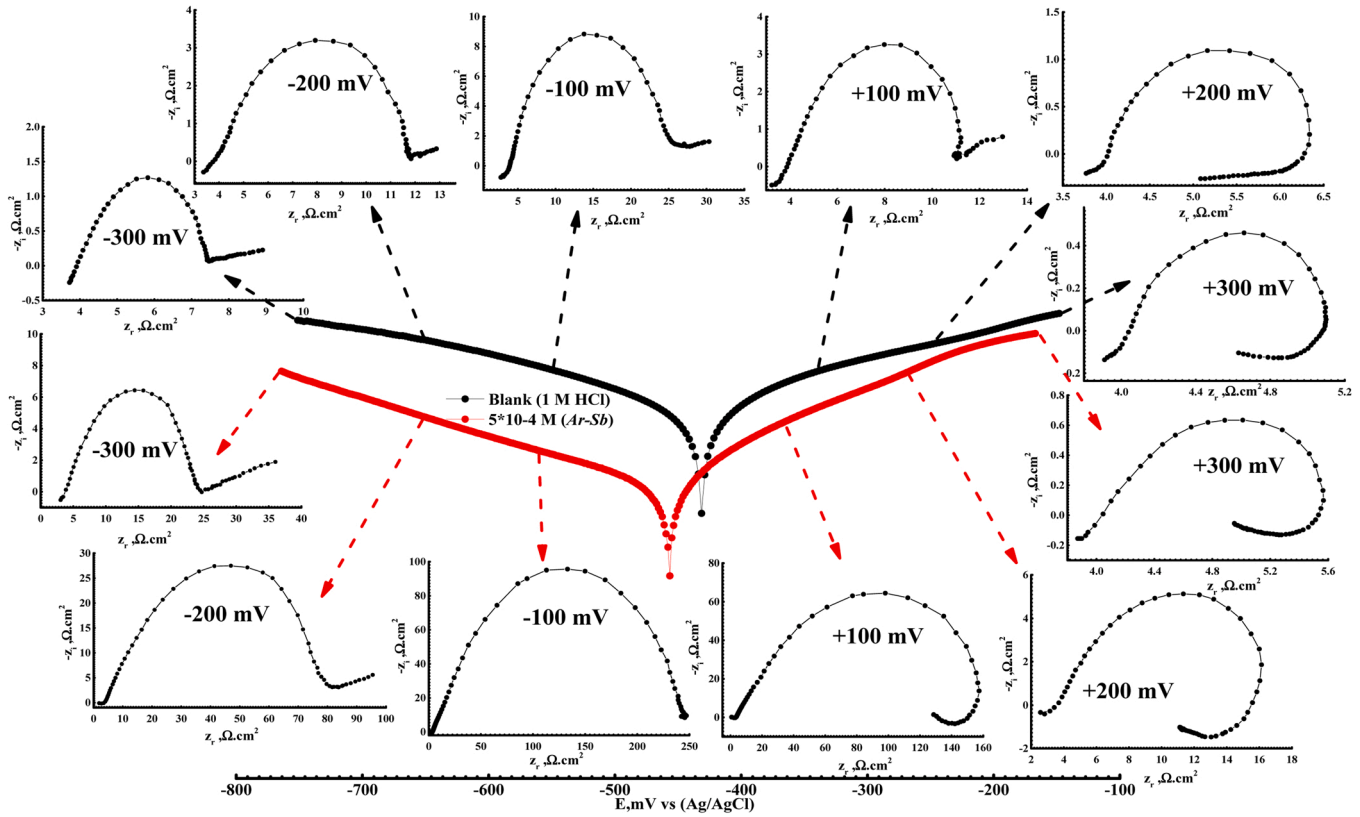

Fig. 11. Nyquist diagrams for *CS* at different anodic and cathodic over potentials in 1 M HCl free and containing 5×10^{-4} M of *Ar-Sb*.

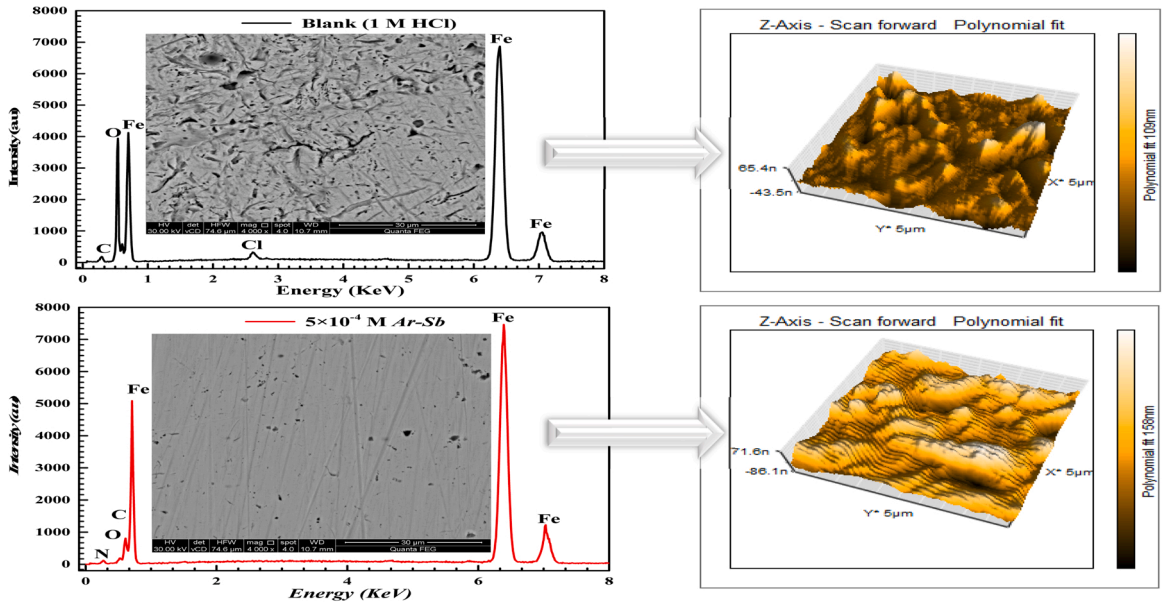

Fig. 12. SEM, EDX and AFM for *CS* in 1 M HCl free and containing 5×10^{-4} M of *Ar-Sb* after 6 h immersion.

value reveals that, *Ar-Sb* molecules react with *CS* surface more easily [92]. ΔN value of the studied *Ar-Sb* (< 3.6) reveals the ability of *Ar-Sb* to donate electrons to the vacant 3d-orbital of Fe[86] while $E_{b\rightarrow d}$ value reflects, tendency of *Ar-Sb* inhibitor to acquire electrons from *CS*[93]. The previously discussed quantum indices were also calculated in liquid phase and listed in Table 8 suggest the higher adsorption probability of the studied *Ar-Sb* inhibitor compared with those calculated in gas phase.

3.5.2. Monte Carlo simulation

MCs is as a highly supportive method for prediction the adsorption of the studied *Ar-Sb* over Fe (110) surface as a corrosion inhibitor. Fig. 10 represents the top and side views of the adsorbed *Ar-Sb* on Fe surface (110) in both gas and liquid phase indicated that, *Ar-Sb* is situated in parallel orientation to *CS* surface. This observation reflects the adsorption ability of the studied *Ar-Sb* and the high surface coverage of *CS* with the adsorbed *Ar-Sb* and therefore decrease the corrosion process [11, 94]. The parallel position of the adsorbed *Ar-Sb* over *CS* surface allows the active centers to react with the Fe surface effectively and offers high protection of *CS* from the aggressive HCl [9,10]. The output data extracted form MCs in Table 9 in both gas and liquid phases give an indication about the interaction between *Ar-Sb* and Fe (110). E_{ads} (adsorption energy) can be defined as the energy released upon *Ar-Sb* binding "relaxed" on *CS* surface. The obtained E_{ads} value in Table 9 of *Ar-Sb* inhibitor in liquid phase (−22332.56 kJ/mol) was found too low compared with that in gas phase (−317.85 kJ/mol), indicating the strong spontaneous adsorption of the studied *Ar-Sb* molecules over *CS* surface. Also, the E_{ads} value of the studied *Ar-Sb* decreases in the order of *Ar-Sb* < Cl^- < H_3O^+ < H_2O. This trend indicates that *Ar-Sb* molecules can effectively replace corrosion particles to form a thermodynamically stable adsorption film on *CS* surface produce a better adsorption effect compared with the pure inhibitors [37,81]. While E_{ads} value decreased in presence of water molecules which is associated with intermolecular HB interactions between *Ar-Sb* and water molecules that enhanced its adsorption on *CS* surface[95]. This observation reflected the key role of the studied inhibitor in *CS* protection by formation of a protective film through the replacement process of the corrosive particles with *Ar-Sb* molecules which suppress the corrosion probability occurrence[96]. The output data extracted form MCs in liquid phase suggested the higher adsorption probability of *Ar-Sb* inhibitor on *CS* surface compared with that in isolated phase (gas phase)[97,98]. The data obtained from MCs was matched with DFT calculated parameters and suggest the inhibition ability of the studied *Ar-Sb* for *CS*.

3.6. Potential zero charge

For more information about the anodic and cathodic reaction mechanism of *CS* surface, EIS technique was applied to explain the PZC of the *CS* in 1 M HCl and after the addition of 5×10^{-4} of *Ar-Sb* at various anodic and cathodic overpotentials (η) which was represented in Nyquist diagrams as seen in Fig. 11. At cathodic range, it can be seen that, Nyquist plots of *CS* in free HCl with two-time constants at − 300 mV, − 200 mV and − 100 mV. The 1st capacitive loop at high frequency was according to R_P, while at low frequency, a straight line appears which can be attributed to accumulated corrosion products at *CS* surface, which hinders the ions diffusion[99]. The same behavior at − 300 mV, − 200 mV was observed after the addition of *Ar-Sb* in which Nyquist diagram comprise two-time constants. The 1st loop was due to R_P and the 2nd was to film resistance[100]. These observations reflected that the H_2 evolution mechanism not affected after the addition of *Ar-Sb* at − 300 mV, − 200 mV[58]. While at − 100 mV in presence of *Ar-Sb*, one time constant (one capacitive loop) was observed [25]. R_P values of *CS* in 1 M HCl were 7.26 Ω.cm^2, 11.83 Ω.cm^2 and 24.14 Ω.cm^2 at cathodic over potential − 300 mV, − 200 mV and − 100 mV respectively, while R_P values of *CS* at the same over potentials after the addition of *Ar-Sb* were 25.19 Ω.cm^2, 80.12 Ω.cm^2 and 254.22 Ω.cm^2 respectively. This exhibited the adsorption capacity of *Ar-Sb* molecules over *CS* surface and reflected that the available surface area for H^+ ions decreases[101].

At anodic range, Nyquist plots of *CS* in 1 M HCl with two-time constants (capacitive loop and straight line) at + 100 mV was observed while after the addition of *Ar-Sb*, a different behavior was observed as seen in Fig. 11. A capacitive loop at higher and medium frequency was observed with the existence of inductive loop at low frequency which can be attributed to the relaxation process of *Ar-Sb* film over *CS* surface [102], [58]. At + 200 mV and + 300 mV, Nyquist plots of *CS* in absence and presence of *Ar-Sb* appeared as a capacitive loop at high frequency followed by an inductive loop at low frequency which can be attributed to the adsorbed intermediate product $((FeCl^-)_{ads})$ formed during *CS* dissolution or adsorbed *Ar-Sb* species over *CS* surface [66,100].

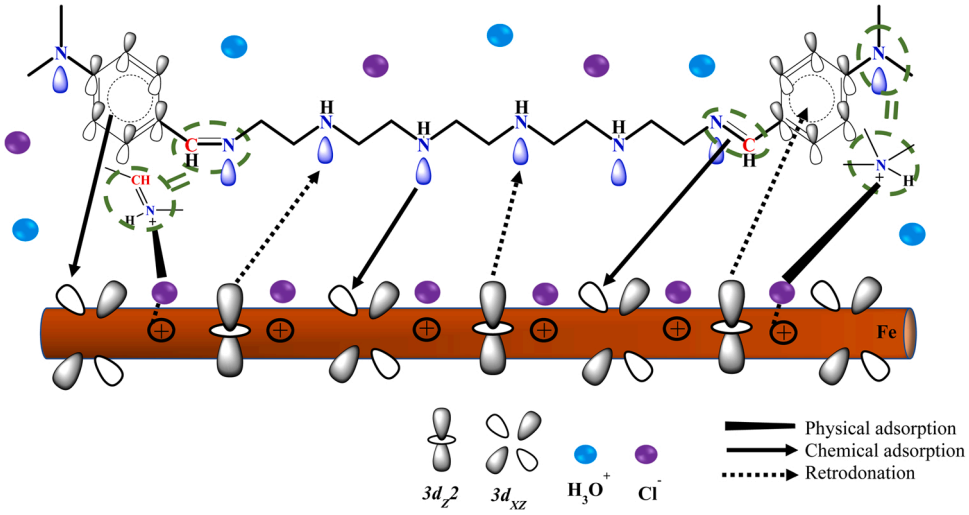

Fig. 13. Suggested adsorption mechanism of *Ar-Sb* over *CS* surface.

3.7. Surface analysis

CS surface was analyzed using SEM photomicrograph analysis which consider a powerful tool parallel to electrochemical measurements (EMs) showing the destructive action of corrosive media (1 M HCl) and the mitigation role of *Ar-Sb* for *CS* after immersion time (6 h) as 2D images as shown in Fig. 12. SEM images reflected the mitigation process of the untreated *CS* in 1 M HCl with highly damaged surface with corrosion products due to the destructive effect of acidic HCl[55,103]. The anticorrosion behavior of *Ar-Sb* was confirmed using 5×10^{-4} M as seen in Fig. 12 which displays tangibly improved *CS* surface smoother than that in the untreated solution (1 M HCl) and free somewhat from corrosion products (Iron oxides and chlorides). This modification proves the shielding of *CS* surface with the adsorbed *Ar-Sb* molecules and formation of a protective film barrier from the corrosive particles decreasing the contact between *CS* surface and corrosive HCl[104], [27]. EDX spectra were applied to detect the components percentage (O, Cl^-, C, Fe and N) on *CS* surface in1 M HCl in absence and presence of 5×10^{-4} M of *Ar-Sb* as shown in Fig. 12. In the untreated solution (1 M HCl), weight percentage (wt%) value of O and Cl^- was 14.54% and 0.26% respectively, while the addition of *Ar-Sb* decreased wt% of O to 1.73% and Cl^- was nearly disappeared. Also, wt% of C increased from 2.16% to 7.46% after the addition of *Ar-Sb* to the corrosive media. On the other side, the presence of N peak with wt% 1.24% indicated formation of *Ar-Sb* layer over *CS* surface. EDX analysis showed an enhancement of Fe peak after *Ar-Sb* addition, indicating that *CS* surface become free of corrosion products [83]. Fig. 12 showed 3D images of *CS* surface in uncontrolled environment (1 M HCl) and containing 5×10^{-4} M of *Ar-Sb*. A huge damage in *CS* surface was noticed as a large peaks or waves of hills and valleys due to the destructive effect of HCl with R_a (average roughness) = 35.27 nm [61]. While the effect of *Ar-Sb* in *CS* protection was observed as a more homogeneous *CS* surface comparative to that in HCl free with R_a= 16.53 nm[105]. These observations reinforced defensive film formation of *Ar-Sb* on *CS* surface that retards the corrosion rate through the adsorption process [95]. The simulated *Ar-Sb* adsorption mechanism over *CS* surface was represented as in Fig. 13 showing various adsorption modes occur during *Ar-Sb* adsorption over *CS* surface.

4. Conclusion

In the present study, a newly aromatic di-imine Schiff base inhibitor (*Ar-Sb*) based on Polyethyleneamines was laboratory synthesized and evaluated as corrosion inhibitor for *CS* in aggressive 1 M HCl solution via different EMs which reflected the mitigation potency of *Ar-Sb* and its role in *CS* protection. PDP measurements exhibited that *Ar-Sb* retard *CS* corrosion by blocking both the anodic and cathodic sites which suggested mixed inhibition (anodic and cathodic) of *Ar-Sb*. Also, EIS showed that R_P of *CS* enhanced after the addition of *Ar-Sb* till reached 497.38 $\Omega.cm^2$ at 5×10^{-4} M with inhibition efficiency 94.33% indicating that the dissolution of *CS* become more difficult in presence of *Ar-Sb* consequently decrease the corrosion rate. The inhibition performance of *Ar-Sb* was studied using various EMs at harsh conditions (various temperature and immersion time) indicating that *Ar-Sb* adsorbed over *CS* surface forming a stable protective layer suggesting that the adsorption of *Ar-Sb* on *CS* was chemically according to Langmuir adsorption isotherm. SEM, EDX and AFM analysis confirmed *CS* protection in presence of *Ar-Sb* and formation of barrier adsorption layer of *Ar-Sb* on *CS* surface. DFT and MCs data showed good correlation with the experimental results and give more information about the reactivity of *Ar-Sb* and its probability to act as efficient corrosion inhibitor.

CRediT authorship contribution statement

Abdelhamed samar: Investigation, Methodology, Supervision, Writing – review & editing. **El-Sharkawy El-sayed:** Investigation, Methodology, Supervision, Writing – original draft. **Mohamed Shaimaa Khalaf:** Investigation, Methodology, Supervision, Writing – review & editing. **Qasim Khaled Faisal:** Data curation, Methodology, Supervision, Writing – original draft. **Elaraby Ahmed:** Data curation, Investigation, Methodology, Supervision, Writing – original draft, Writing – review & editing.

Declaration of Competing Interest

The authors declare no competing interests.

Data Availability

Data will be made available on request.

Acknowledgments

The authors grateful to Faculty of Science (Suez University), Faculty of Engineering at Shoubra (Benha University) and Egyptian Petroleum Research Institute (EPRI) for their support.

Appendix A. Supporting information

Supplementary data associated with this article can be found in the online version at doi:10.1016/j.jece.2023.111861.

References

[1] S. Javadian, B. Darbasizadeh, A. Yousefi, F. Ektefa, N. Dalir, J. Kakemam, Dye-surfactant aggregates as corrosion inhibitor for mild steel in NaCl medium: Experimental and theoretical studies, J. Taiwan Inst. Chem. Eng. 71 (2017) 344–354, https://doi.org/10.1016/j.jtice.2016.11.014.

[2] S.A. Jafar, A.A. Aabid, J.I. Humadi, Corrosion behavior of carbon steel in 1 M, 2 M, and 3 M HCl solutions, Mater. Today Proc. (2021) 2–7, https://doi.org/10.1016/j.matpr.2021.12.295.

[3] Q.H. Zhang, Y.Y. Li, Y. Lei, X. Wang, H.F. Liu, G.A. Zhang, Comparison of the synergistic inhibition mechanism of two eco-friendly amino acids combined corrosion inhibitors for carbon steel pipelines in oil and gas production, Appl. Surf. Sci. 583 (2022), https://doi.org/10.1016/j.apsusc.2022.152559.

[4] L. Toukal, M. Foudia, D. Haffar, N. Aliouane, M. Al-Noaimi, Y. Bellal, H. Elmsellem, Abdel-Rahman, Monte Carlo simulation and electrochemical performance corrosion inhibition whid benzimidazole derivative for XC48 steel in 0.5 M H2SO4 and 1.0 M HCl solutions, J. Indian Chem. Soc. 99 (2022) 1–11, https://doi.org/10.1016/j.jics.2022.100634.

[5] M. Srivastava, P. Tiwari, S.K. Srivastava, R. Prakash, G. Ji, Electrochemical investigation of Irbesartan drug molecules as an inhibitor of mild steel corrosion in 1 M HCl and 0.5 M H2SO4 solutions, J. Mol. Liq. 236 (2017) 184–197, https://doi.org/10.1016/j.molliq.2017.04.017.

[6] X. Li, S. Deng, H. Fu, Inhibition of the corrosion of steel in HCl, H 2SO 4 solutions by bamboo leaf extract, Corros. Sci. 62 (2012) 163–175, https://doi.org/10.1016/j.corsci.2012.05.008.

[7] M. Corrales-Luna, T. Le Manh, M. Romero-Romo, M. Palomar-Pardavé, E. M. Arce-Estrada, 1-Ethyl 3-methylimidazolium thiocyanate ionic liquid as corrosion inhibitor of API 5L X52 steel in H 2 SO 4 and HCl media, Corros. Sci. 153 (2019) 85–99, https://doi.org/10.1016/j.corsci.2019.03.041.

[8] N.B. Iroha, C.U. Dueke-Eze, T.M. Fasina, V.C. Anadebe, L. Guo, Anticorrosion activity of two new pyridine derivatives in protecting X70 pipeline steel in oil well acidizing fluid: experimental and quantum chemical studies, J. Iran. Chem. Soc. 19 (2022) 2331–2346, https://doi.org/10.1007/s13738-021-02450-2.

[9] M. El Faydy, F. Benhiba, I. Warad, A.S. Abousalem, H. About, Y. Kerroum, C. Jama, A. Guenbour, B. Lakhrissi, A. Zarrouk, Appraisal of corrosion inhibiting ability of new 5-N-((alkylamino)methyl)quinolin-8-ol analogs for C40E steel in sulfuric acid, Int. J. Hydrog. Energy 46 (2021) 30246–30266, https://doi.org/10.1016/j.ijhydene.2021.06.205.

[10] L.O. Olasunkanmi, I.B. Obot, M.M. Kabanda, E.E. Ebenso, Some quinoxalin-6-yl derivatives as corrosion inhibitors for mild steel in hydrochloric acid: Experimental and theoretical studies, J. Phys. Chem. C. 119 (2015) 16004–16019, https://doi.org/10.1021/acs.jpcc.5b03285.

[11] I. Nadi, M. Bouanis, F. Benhiba, K. Nohair, A. Nyassi, A. Zarrouk, C. Jama, F. Bentiss, Insights into the inhibition mechanism of 2,5-bis(4-pyridyl)-1,3,4-oxadiazole for carbon steel corrosion in hydrochloric acid pickling via experimental and computational approaches, J. Mol. Liq. 342 (2021) 116958, https://doi.org/10.1016/j.molliq.2021.116958.

[12] F. Ríos, M. Lechuga, M. Fernández-Serrano, A. Fernández-Arteaga, Aerobic biodegradation of amphoteric amine-oxide-based surfactants: Effect of molecular structure, initial surfactant concentration and pH, Chemosphere 171 (2017) 324–331, https://doi.org/10.1016/j.chemosphere.2016.12.070.

[13] T.D. Prichard, R.R. Thomas, C.M. Kausch, B.D. Vogt, Solubility of non-ionic poly (fluorooxetane)-block-(ethylene oxide)-block-(fluorooxetane) surfactants in carbon dioxide, J. Supercrit. Fluids 57 (2011) 95–100, https://doi.org/10.1016/j.supflu.2011.02.014.

[14] G. Wang, S. Wang, Z. Sun, S. Zheng, Y. Xi, Structures of nonionic surfactant modified montmorillonites and their enhanced adsorption capacities towards a cationic organic dye, Appl. Clay Sci. 148 (2017) 1–10, https://doi.org/10.1016/j.clay.2017.08.001.

[15] E.G. Zaki, T.A. Zidan, Methyl Acrylate Derivatives as Corrosion Inhibitors for X-65 Type Carbon Steel in 1 M HCl 16 (2021), https://doi.org/10.20964/2021.03.23.

[16] W.I. Eldougdoug, A.I. Ali, A. Elaraby, E.M. Mabrouk, Corros. Inhib. Tri-cationic Surfactant Carbon Steel hydrochloric Acid. Solut. 5 (2018) 289–300.

[17] W.I. El-Dougdoug, A.S. Al-Gorair, A. Abou Elsaoud, H. Hawsawi, A. Elaraby, E. S. Mabrouk, M. Abdallah, Synthesis and assessment of Gemini cationic surfactants as inhibitors for corrosion of carbon steel in hydrochloric acid, Green. Chem. Lett. Rev. 15 (2022) 796–812, https://doi.org/10.1080/17518253.2022.2135389.

[18] S. Cao, D. Liu, H. Ding, J. Wang, H. Lu, J. Gui, Task-specific ionic liquids as corrosion inhibitors on carbon steel in 0.5 M HCl solution: An experimental and theoretical study, Corros. Sci. 153 (2019) 301–313, https://doi.org/10.1016/j.corsci.2019.03.035.

[19] P. Kannan, J. Karthikeyan, P. Murugan, T.S. Rao, N. Rajendran, Corrosion Inhibition effect of novel methyl benzimidazolium Ionic liquid for carbon steel in HCl medium, J. Mol. Liq. 221 (2016) 368–380, https://doi.org/10.1016/j.molliq.2016.04.130.

[20] S. Du, S. Chen, Z. Zhang, Z. Ye, H. Mao, H. Yang, C. Lian, C. Bao, Corrosion inhibition behavior of hydroxyl-terminated hyperbranched poly(amine-ester) for Q235 steel in HCl solution, Mater. Chem. Phys. 292 (2022) 126831, https://doi.org/10.1016/j.matchemphys.2022.126831.

[21] N. Punitha, R. Ganapathi Sundaram, K. Vijayalakshmi, R. Rengasamy, J. Elangovan, Interactions and corrosion mitigation prospective of pyrazole derivative on mild steel in HCl environment, J. Indian Chem. Soc. 99 (2022) 100667, https://doi.org/10.1016/j.jics.2022.100667.

[22] V.C. Anadebe, V.I. Chukwuike, K. Chandra Nayak, E.E. Ebenso, R. Chandra Barik, Combined electrochemical, atomic scale-DFT and MD simulation of Nickel based metal organic framework (Ni-MOF) as corrosion inhibitor for X65 pipeline steel in CO_2- saturated brine, Mater. Chem. Phys. 312 (2024) 128606, https://doi.org/10.1016/j.matchemphys.2023.128606.

[23] V.C. Anadebe, V.I. Chukwuike, V. Selvaraj, A. Pandikumar, R.C. Barik, Sulfur-doped graphitic carbon nitride (S-g-C3N4) as an efficient corrosion inhibitor for X65 pipeline steel in CO_2- saturated 3.5% NaCl solution: Electrochemical, XPS and Nanoindentation Studies, Process Saf. Environ. Prot. 164 (2022) 715–728, https://doi.org/10.1016/j.psep.2022.06.055.

[24] M.A. Bedair, S.A. Soliman, M.F. Bakr, E.S. Gad, H. Lgaz, I.M. Chung, M. Salama, F. Z. Alqahtany, Benzidine-based Schiff base compounds for employing as corrosion inhibitors for carbon steel in 1.0 M HCl aqueous media by chemical, electrochemical and computational methods, J. Mol. Liq. 317 (2020) 114015, https://doi.org/10.1016/j.molliq.2020.114015.

[25] M. Salim, M.M. Azab, M.A. Abo-Riya, M. Abd-El-Raouf, N.M. EL Basiony, Controlling C-steel dissolution in 1 M HCl solution using newly synthesized ρ-substituted imine derivatives: Theoretical (DFT and MCs) and experimental investigations, J. Mol. Struct. 1274 (2023) 134357, https://doi.org/10.1016/j.molstruc.2022.134357.

[26] M. Murmu, S.K. Saha, N.C. Murmu, P. Banerjee, Effect of stereochemical conformation into the corrosion inhibitive behaviour of double azomethine based Schiff bases on mild steel surface in 1 mol L−1 HCl medium: an experimental, density functional theory and molecular dynamics simulation study, Corros. Sci. 146 (2019) 134–151, https://doi.org/10.1016/j.corsci.2018.10.002.

[27] X. Li, L. Chen, B. Xie, C. Lai, J. He, J. Feng, Y. Yang, R. Ji, M. Liu, Two semi flexible nonplanar double Schiff bases as corrosion inhibitors for mild steel in HCl solution: Experimental and theoretical investigations, J. Environ. Chem. Eng. 11 (2023) 110077, https://doi.org/10.1016/j.jece.2023.110077.

[28] N.M. El Basiony, E.E. Badr, S.A. Baker, A.S. El-Tabei, Experimental and theoretical (DFT&MC) studies for the adsorption of the synthesized Gemini cationic surfactant based on hydrazide moiety as X-65 steel acid corrosion inhibitor, Appl. Surf. Sci. 539 (2021) 148246, https://doi.org/10.1016/j.apsusc.2020.148246.

[29] K. Zakaria, M.A. Abbas, M.A. Bedair, Herbal expired drug bearing glycosides and polysaccharides moieties as green and cost-effective oilfield corrosion inhibitor: Electrochemical and computational studies, J. Mol. Liq. 352 (2022) 118689, https://doi.org/10.1016/j.molliq.2022.118689.

[30] C.U. Dueke-Eze, N.A. Madueke, N.B. Iroha, N.J. Maduelosi, L.A. Nnanna, V. C. Anadebe, A.A. Chokor, Adsorption and inhibition study of N-(5-methoxy-2-hydroxybenzylidene) isonicotinohydrazide Schiff base on copper corrosion in 3.5% NaCl, Egypt. J. Pet. 31 (2022) 31–37, https://doi.org/10.1016/j.ejpe.2022.05.001.

[31] F. Kaya, R. Solmaz, İ.H. Geçibesler, Adsorption and corrosion inhibition capability of Rheum ribes root extract (Işgın) for mild steel protection in acidic medium: A comprehensive electrochemical, surface characterization, synergistic inhibition effect, and stability study, J. Mol. Liq. 372 (2023), https://doi.org/10.1016/j.molliq.2023.121219.

[32] D.M. Ragheb, A.M. Abdel-Gaber, F.M. Mahgoub, M.E. Mohamed, Eco-friendly method for construction of superhydrophobic graphene-based coating on copper substrate and its corrosion resistance performance, Sci. Rep. 12 (1) (2022) 14, https://doi.org/10.1038/s41598-022-22915-5.

[33] A.S. El-Tabei, O.E. El-Azabawy, N.M. El Basiony, M.A. Hegazy, Newly synthesized quaternary ammonium bis-cationic surfactant utilized for mitigation of carbon steel acidic corrosion; theoretical and experimental investigations, J. Mol. Struct. 1262 (2022) 133063, https://doi.org/10.1016/j.molstruc.2022.133063.

[34] M. Mobin, R. Aslam, Experimental and theoretical study on corrosion inhibition performance of environmentally benign non-ionic surfactants for mild steel in 3.5% NaCl solution, Process Saf. Environ. Prot. 114 (2018) 279–295, https://doi.org/10.1016/j.psep.2018.01.001.

[35] S.M. Shaban, M.F. Elbhrawy, A.S. Fouda, S.M. Rashwan, H.E. Ibrahim, A. M. Elsharif, Corrosion inhibition and surface examination of carbon steel 1018 via N-(2-(2-hydroxyethoxy)ethyl)-N,N-dimethyloctan-1-aminium bromide in 1.0 M HCl, J. Mol. Struct. 1227 (2021) 129713, https://doi.org/10.1016/j.molstruc.2020.129713.

[36] W. Luo, Q. Lin, X. Ran, W. Li, B. Tan, A. Fu, S. Zhang, A new pyridazine derivative synthesized as an efficient corrosion inhibitor for copper in sulfuric acid medium: Experimental and theoretical calculation studies, J. Mol. Liq. 341 (2021) 117370, https://doi.org/10.1016/j.molliq.2021.117370.

[37] E. Berdimurodov, A. Kholikov, K. Akbarov, L. Guo, A.M. Abdullah, M. Elik, A gossypol derivative as an efficient corrosion inhibitor for St2 steel in 1 M HCl + 1 M KCl: An experimental and theoretical investigation, J. Mol. Liq. 328 (2021), https://doi.org/10.1016/j.molliq.2021.115475.

[38] F. Kaya, R. Solmaz, The use of methanol extract of Rheum Ribes (Is ß gın) flower as a natural and promising corrosion inhibitor for mild steel protection in 1 M HCl solution, J. Ind. Eng. Chem. 122 (2023) 102–117, https://doi.org/10.1016/j.jiec.2023.02.013.

[39] A.R. Shahmoradi, M. Ranjbarghanei, A.A. Javidparvar, L. Guo, E. Berdimurodov, B. Ramezanzadeh, Theoretical and surface/electrochemical investigations of walnut fruit green husk extract as effective inhibitor for mild-steel corrosion in

1M HCl electrolyte, J. Mol. Liq. 338 (2021) 116550, https://doi.org/10.1016/j.molliq.2021.116550.
[40] R. Solmaz, A. Salcı, Y.A. Dursun, G. Kardaş, A comprehensive study on the adsorption, corrosion inhibition efficiency and stability of acriflavine on mild steel in 1 M HCl solution, Colloids Surf. A Physicochem. Eng. Asp. 674 (2023), https://doi.org/10.1016/j.colsurfa.2023.131908.
[41] M. Mobin, R. Aslam, R. Salim, S. Kaya, An investigation on the synthesis, characterization and anti-corrosion properties of choline based ionic liquids as novel and environmentally friendly inhibitors for mild steel corrosion in 5% HCl, J. Colloid Interface Sci. 620 (2022) 293–312, https://doi.org/10.1016/j.jcis.2022.04.036.
[42] E. Berdimurodov, A. Kholikov, K. Akbarov, L. Guo, S. Kaya, D.K. Verma, M. Rbaa, O. Dagdag, Novel glycoluril pharmaceutically active compound as a green corrosion inhibitor for the oil and gas industry, J. Electroanal. Chem. 907 (2022), https://doi.org/10.1016/j.jelechem.2022.116055.
[43] A.S. El-Tabei, A.E. El-Tabey, N.M. El Basiony, Newly imine-azo dicationic amphiphilic for corrosion and sulfate-reducing bacteria inhibition in petroleum processes: Laboratory and theoretical studies, Appl. Surf. Sci. 573 (2022) 151531, https://doi.org/10.1016/j.apsusc.2021.151531.
[44] A. Döner, G. Kardaş, N-Aminorhodanine as an effective corrosion inhibitor for mild steel in 0.5M H2SO4, Corros. Sci. 53 (2011) 4223–4232, https://doi.org/10.1016/j.corsci.2011.08.032.
[45] A.S. El-Tabei, A.E. El-Tabey, N.M. El Basiony, Newly imine-azo dicationic amphiphilic for corrosion and sulfate-reducing bacteria inhibition in petroleum processes: laboratory and theoretical studies, Appl. Surf. Sci. 573 (2022) 151531, https://doi.org/10.1016/j.apsusc.2021.151531.
[46] M. Abdallah, H.M. Eltass, M.A. Hegazy, H. Ahmed, Adsorption and inhibition effect of novel cationic surfactant for pipelines carbon steel in acidic solution, Prot. Met. Phys. Chem. Surf. 52 (2016) 721–730, https://doi.org/10.1134/S207020511604002X.
[47] N.M. El Basiony, A. Elgendy, A.E. El-Tabey, A.M. Al-Sabagh, G.M. Abd El-Hafez, M.A. El-raouf, M.A. Migahed, Synthesis, characterization, experimental and theoretical calculations (DFT and MC) of ethoxylated aminothiazole as inhibitor for X65 steel corrosion in highly aggressive acidic media, J. Mol. Liq. 297 (2020) 111940, https://doi.org/10.1016/j.molliq.2019.111940.
[48] R. Haldhar, C. Jayprakash Raorane, V.K. Mishra, T. Periyasamy, A. Berisha, S. C. Kim, Development of different chain lengths ionic liquids as green corrosion inhibitors for oil and gas industries: Experimental and theoretical investigations, J. Mol. Liq. 372 (2023) 121168, https://doi.org/10.1016/j.molliq.2022.121168.
[49] A. Elaraby, A. Elgendy, M.A. Migahed, A.M. Abdullah, S.M. Alharbi, S.M. Shaban, D.H. Kim, N.M. El Basiony, Synthesis of Gemini cationic surfactants based on natural nicotinic acid and evaluation of their inhibition performance at C-steel/1M HCl interface_ Electrochemical and computational investigations, Colloids Surf. A Physicochem. Eng. Asp. (2022) 130687, https://doi.org/10.1016/j.colsurfa.2022.130687.
[50] A. Khadiri, A. Ousslim, K. Bekkouche, A. Aouniti, I. Warad, A. Elidrissi, B. Hammouti, F. Bentiss, M. Bouachrine, A. Zarrouk, 4-(2-(2-(2-(2-(Pyridine-4-yl) ethylthio)ethoxy)ethylthio)ethyl)pyridine as new corrosion inhibitor for mild steel in 1.0 M HCl solution: experimental and theoretical studies, J. Bio- Tribo-Corros. 4 (2018) 1–18, https://doi.org/10.1007/s40735-018-0179-3.
[51] O. Kaczerewska, R. Leiva-garcia, R. Akid, B. Brycki, Ef fi ciency of cationic gemini surfactants with 3-azamethylpentamethylene spacer as corrosion inhibitors for stainless steel in hydrochloric acid, J. Mol. Liq. 247 (2017) 6–13, https://doi.org/10.1016/j.molliq.2017.09.103.
[52] R. Aslam, M. Mobin, J. Aslam, H. Lgaz, I.M. Chung, Inhibitory effect of sodium carboxymethylcellulose and synergistic biodegradable gemini surfactants as effective inhibitors for MS corrosion in 1 M HCl, J. Mater. Res. Technol. 8 (2019) 4521–4533, https://doi.org/10.1016/j.jmrt.2019.07.065.
[53] M. Pakiet, I. Kowalczyk, R. Leiva Garcia, R. Akid, B. Brycki, Cationic clevelable surfactants as highly efficient corrosion inhibitors of stainless steel AISI 304: electrochemical study, J. Mol. Liq. 315 (2020), https://doi.org/10.1016/j.molliq.2020.113675.
[54] X. Jin, J. Wang, S. Zheng, J. Li, X. Ma, L. Feng, H. Zhu, Z. Hu, The study of surface activity and anti-corrosion of novel surfactants for carbon steel in 1 M HCl, J. Mol. Liq. 353 (2022) 118747, https://doi.org/10.1016/j.molliq.2022.118747.
[55] A.S. El-Tabei, M.A. Hegazy, A.H. Bedair, N.M. El Basiony, M.A. Sadeq, Novel macrocyclic cationic surfactants: Synthesis, experimental and theoretical studies of their corrosion inhibition activity for carbon steel and their antimicrobial activities, J. Mol. Liq. 345 (2022) 116990, https://doi.org/10.1016/j.molliq.2021.116990.
[56] N.M. El Basiony, M.A. Hegazy, Newly synthesized quaternary ammonium bis-cationic surfactant utilized for mitigation of carbon steel acidic corrosion; theoretical and experimental investigations, J. Mol. Struct. 1262 (2022) 133063, https://doi.org/10.1016/j.molstruc.2022.133063.
[57] B. Sargolzaei, A. Arab, Synergism of CTAB and NLS surfactants on the corrosion inhibition of mild steel in sodium chloride solution, Mater. Today Commun. 29 (2021) 102809, https://doi.org/10.1016/j.mtcomm.2021.102809.
[58] R. Solmaz, G. Kardaş, M. Çulha, B. Yazici, M. Erbil, Investigation of adsorption and inhibitive effect of 2-mercaptothiazoline on corrosion of mild steel in hydrochloric acid media, Electrochim. Acta 53 (2008) 5941–5952, https://doi.org/10.1016/j.electacta.2008.03.055.
[59] A.S. El-Tabei, M.A. Hegazy, A.H. Bedair, M.A. Sadeq, Synthesis and inhibition effect of a novel Tri-cationic surfactant on carbon steel corrosion in 0.5 M H2SO4 solution, J. Surfactants Deterg. 17 (2014) 341–352, https://doi.org/10.1007/s11743-013-1524-7.
[60] A.S. El-Tabei, O.E. El-Azabawy, N.M. El Basiony, M.A. Hegazy, Newly synthesized quaternary ammonium bis-cationic surfactant utilized for mitigation of carbon steel acidic corrosion; theoretical and experimental investigations, J. Mol. Struct. 1262 (2022) 133063, https://doi.org/10.1016/j.molstruc.2022.133063.
[61] T. Zheng, J. Liu, M. Wang, Q. Liu, J. Wang, Y. Chong, G. Jia, Synergistic corrosion inhibition effects of quaternary ammonium salt cationic surfactants and thiourea on Q235 steel in sulfuric acid: Experimental and theoretical research, Corros. Sci. 199 (2022) 110199, https://doi.org/10.1016/j.corsci.2022.110199.
[62] F. Bentiss, M. Lebrini, M. Lagrenée, Thermodynamic characterization of metal dissolution and inhibitor adsorption processes in mild steel/2, 5-bis (n-thienyl)-1, 3, 4-thiadiazoles/hydrochloric acid system, Corros. Sci. 47 (2005) 2915–2931.
[63] A.S. Fouda, H.E. Megahed, N. Fouad, N.M. Elbahrawi, Corrosion inhibition of carbon steel in 1 M hydrochloric acid solution by aqueous extract of thevetia peruviana, J. Bio- Tribo-Corros. 2 (2016) 1–13, https://doi.org/10.1007/s40735-016-0046-z.
[64] A.M. Al-Sabagh, M.A. Migahed, S.A. Sadeek, N.M. El Basiony, Inhibition of mild steel corrosion and calcium sulfate formation in highly saline synthetic water by a newly synthesized anionic carboxylated surfactant, Egypt. J. Pet. 27 (2018) 811–821, https://doi.org/10.1016/j.ejpe.2017.12.003.
[65] A. Elaraby, A. Elgendy, M. Abd-El-Raouf, M.A. Migahed, A.S. El-Tabei, A. M. Abdullah, N.H. Al-Qahtani, S.M. Alharbi, S.M. Shaban, D.H. Kim, N.M. El Basiony, Synthesis of gemini cationic surfactants based on natural nicotinic acid and evaluation of their inhibition performance at C-steel/1 M HCl interface: electrochemical and computational investigations, Colloids Surf. A Physicochem. Eng. Asp. 659 (2023) 130687, https://doi.org/10.1016/j.colsurfa.2022.130687.
[66] M. Palomar-Pardavé, M. Romero-Romo, H. Herrera-Hernández, M.A. Abreu-Quijano, N.V. Likhanova, J. Uruchurtu, J.M. Juárez-García, Influence of the alkyl chain length of 2 amino 5 alkyl 1,3,4 thiadiazole compounds on the corrosion inhibition of steel immersed in sulfuric acid solutions, Corros. Sci. 54 (2012) 231–243, https://doi.org/10.1016/j.corsci.2011.09.020.
[67] Y. Fu L. Liu H. Yu Y. Wang Q. Guo. Quantum-Chem. Predict. Absol. Stand. Redox Potentials Divers. Org. Mol. Free Radic. Acetonitrile 2005 7227 7234.
[68] M.A. Deyab, S.T. Keera, Cyclic voltammetric studies of carbon steel corrosion in chloride-formation water solution and effect of some inorganic salts, Egypt. J. Pet. 21 (2012) 31–36, https://doi.org/10.1016/j.ejpe.2012.02.005.
[69] A. Salcı, H. Yüksel, R. Solmaz, Experimental studies on the corrosion inhibition performance of 2-(2-aminophneyl)benzimidazole for mild steel protection in 1 M HCl solution, J. Taiwan Inst. Chem. Eng. 134 (2022), https://doi.org/10.1016/j.jtice.2022.104349.
[70] M. Mobin, M. Parveen, Huda, R. Aslam, Effect of different additives, temperature, and immersion time on the inhibition behavior of L-valine for mild steel corrosion in 5% HCl solution, J. Phys. Chem. Solids 161 (2022) 110422, https://doi.org/10.1016/j.jpcs.2021.110422.
[71] M. Mobin, R. Aslam, J. Aslam, Non toxic biodegradable cationic gemini surfactants as novel corrosion inhibitor for mild steel in hydrochloric acid medium and synergistic effect of sodium salicylate: Experimental and theoretical approach, Mater. Chem. Phys. 191 (2017) 151–167, https://doi.org/10.1016/j.matchemphys.2017.01.037.
[72] M. El Faydy, R. Touir, M. Ebn Touhami, A. Zarrouk, C. Jama, B. Lakhrissi, L. O. Olasunkanmi, E.E. Ebenso, F. Bentiss, Corrosion inhibition performance of newly synthesized 5-alkoxymethyl-8-hydroxyquinoline derivatives for carbon steel in 1 M HCl solution: Experimental, DFT and Monte Carlo simulation studies, Phys. Chem. Chem. Phys. 20 (2018) 20167–20187, https://doi.org/10.1039/c8cp03226b.
[73] M.A. Gebril, M.A. Bedair, S.A. Soliman, M.F. Bakr, M. Basseem, I. Mohamed, Experimental and computational studies of the influence of non-ionic surfactants with coumarin moiety as corrosion inhibitors for carbon steel in 1. 0 M HCl, J. Mol. Liq. 349 (2022) 118445, https://doi.org/10.1016/j.molliq.2021.118445.
[74] G. Xia, X. Jiang, L. Zhou, Y. Liao, M. Duan, H. Wang, Q. Pu, J. Zhou, Enhanced anticorrosion of methyl acrylate by covalent bonded N-alkylpyridinium bromide for X70 steel in 5M HCl, J. Ind. Eng. Chem. 27 (2015) 133–148, https://doi.org/10.1016/j.jiec.2014.12.027.
[75] F.M. Mahgoub, B.A. Abdel-Nabey, Y.A. El-Samadisy, Adopting a multipurpose inhibitor to control corrosion of ferrous alloys in cooling water systems, Mater. Chem. Phys. 120 (2010) 104–108, https://doi.org/10.1016/j.matchemphys.2009.10.028.
[76] F. Bentiss, F. Gassama, D. Barbry, L. Gengembre, H. Vezin, M. Lagrenée, M. Traisnel, Enhanced corrosion resistance of mild steel in molar hydrochloric acid solution by 1,4-bis(2-pyridyl)-5H-pyridazino[4,5-b]indole: electrochemical, theoretical and XPS studies, Appl. Surf. Sci. 252 (2006) 2684–2691, https://doi.org/10.1016/j.apsusc.2005.03.231.
[77] F. Zhang, Y. Tang, Z. Cao, W. Jing, Z. Wu, Y. Chen, Performance and theoretical study on corrosion inhibition of 2-(4-pyridyl)-benzimidazole for mild steel in hydrochloric acid, Corros. Sci. 61 (2012) 1–9, https://doi.org/10.1016/j.corsci.2012.03.045.
[78] C. Wang, C. Zou, Y. Cao, Electrochemical and isothermal adsorption studies on corrosion inhibition performance of β-cyclodextrin grafted polyacrylamide for X80 steel in oil and gas production, J. Mol. Struct. 1228 (2021) 129737, https://doi.org/10.1016/j.molstruc.2020.129737.
[79] A.H. Tantawy, K.A. Soliman, H.M. Abd El-Lateef, Novel synthesized cationic surfactants based on natural Piper nigrum as sustainable-green inhibitors for steel pipeline corrosion in CO_2-3.5%NaCl: DFT, Monte Carlo simulations and experimental approaches, J. Clean. Prod. 250 (2020) 119510, https://doi.org/10.1016/j.jclepro.2019.119510.

[80] R. Yildiz, A. Döner, T. Doğan, I. Dehri, Experimental studies of 2-pyridinecarbonitrile as corrosion inhibitor for mild steel in hydrochloric acid solution, Corros. Sci. 82 (2014) 125–132, https://doi.org/10.1016/j.corsci.2014.01.008.
[81] E. Berdimurodov, D.K. Verma, A. Kholikov, K. Akbarov, L. Guo, The recent development of carbon dots as powerful green corrosion inhibitors: A prospective review, J. Mol. Liq. 349 (2022) 118124, https://doi.org/10.1016/j.molliq.2021.118124.
[82] E. Berdimurodov, A. Kholikov, K. Akbarov, L. Guo, S. Kaya, K.P. Katin, D. K. Verma, M. Rbaa, O. Dagdag, R. Haldhar, Novel gossypol–indole modification as a green corrosion inhibitor for low–carbon steel in aggressive alkaline–saline solution, Colloids Surf. A Physicochem. Eng. Asp. 637 (2022), https://doi.org/10.1016/j.colsurfa.2021.128207.
[83] R. Hsissou, S. Abbout, A. Berisha, M. Berradi, M. Assouag, N. Hajjaji, A. Elharfi, Experimental, DFT and molecular dynamics simulation on the inhibition performance of the DGDCBA epoxy polymer against the corrosion of the E24 carbon steel in 1.0 M HCl solution, J. Mol. Struct. 1182 (2019) 340–351, https://doi.org/10.1016/j.molstruc.2018.12.030.
[84] V. Mehmeti, F.I. Podvorica, Experimental and theoretical studies on corrosion inhibition of niobium and tantalum surfaces by carboxylated graphene oxide, Materials 11 (2018), https://doi.org/10.3390/ma11060893.
[85] A. Molhi, R. Hsissou, M. Damej, A. Berisha, V. Thaçi, A. Belafhaili, M. Benmessaoud, N. Labjar, S. El Hajjaji, Contribution to the corrosion inhibition of c38 steel in 1 m hydrochloric acid medium by a new epoxy resin pgeppp, Int. J. Corros. Scale Inhib. 10 (2021) 399–418, https://doi.org/10.17675/2305-6894-2021-10-1-23.
[86] A. Elaraby, S. Abd, A. Eman, E.G. Zaki, Theoretical and electrochemical evaluation of tetra - cationic surfactant as corrosion inhibitor for carbon steel in 1 M HCl, Sci. Rep. 18 (1) (2023), https://doi.org/10.1038/s41598-023-27513-7.
[87] M. Rahimi, E.B. Noruzi, E. Sheykhsaran, B. Ebadi, Z. Kariminezhad, M. Molaparast, M.G. Mehrabani, B. Mehramouz, M. Yousefi, R. Ahmadi, B. Yousefi, K. Ganbarov, F.S. Kamounah, V. Shafiei-Irannejad, H.S. Kafil, Carbohydrate polymer-based silver nanocomposites: Recent progress in the antimicrobial wound dressings, Carbohydr. Polym. 231 (2020), https://doi.org/10.1016/j.carbpol.2019.115696.
[88] E. Berdimurodov, C. Verma, K. Berdimuradov, M.A. Quraishi, A. Kholikov, K. Akbarov, N. Umirov, B. Borikhonov, 8–Hydroxyquinoline is key to the development of corrosion inhibitors: an advanced review, Inorg. Chem. Commun. 144 (2022) 109839, https://doi.org/10.1016/j.inoche.2022.109839.
[89] Z. Song, S. Donkor, Y. Zhang, Q. Liu, Y. Liu, X. Na, H. Cai, J. Kwesi Odoom, Adsorption and corrosion inhibition performance of rice bran extract on carbon steel in aqueous chloride solution: experimental, computational and theoretical studies, Constr. Build. Mater. 363 (2023), https://doi.org/10.1016/j.conbuildmat.2022.129801.
[90] L. Yang, H. Fan, R. Yan, J. Zhang, S. Liu, X. Huang, D. Zhang, N-substituted methyl ethylenediamine derivatives as corrosion inhibitors for carbon steel in 1 M hydrochloride acid, J. Mol. Struct. 1270 (2022) 133975, https://doi.org/10.1016/j.molstruc.2022.133975.
[91] A.M. Al-Sabagh, N.M. El Basiony, S.A. Sadeek, M.A. Migahed, Scale and corrosion inhibition performance of the newly synthesized anionic surfactant in desalination plants: Experimental, and theoretical investigations, Desalination 437 (2018) 45–58, https://doi.org/10.1016/j.desal.2018.01.036.
[92] A.H. El-Askalany, S.I. Mostafa, K. Shalabi, A.M. Eid, S. Shaaban, Novel tetrazole-based symmetrical diselenides as corrosion inhibitors for N80 carbon steel in 1 M HCl solutions: experimental and theoretical studies, J. Mol. Liq. 223 (2016) 497–508, https://doi.org/10.1016/j.molliq.2016.08.088.
[93] N.M. Elbasiony, Controlling C-steel dissolution in 1M HCl solution using newly synthesized ρ- substituted imine derivatives: theoretical (DFT and MCs) and experimental investigations, J. Mol. Struct. (2022) 134357, https://doi.org/10.1016/j.molstruc.2022.134357.
[94] M. El Faydy, F. Benhiba, I. Warad, H. About, S. Saoiabi, A. Guenbour, F. Bentiss, B. Lakhrissi, A. Zarrouk, Experimental and theoretical investigations of two quinolin-8-ol derivatives as inhibitors for carbon steel in 1 M HCl solution, J. Phys. Chem. Solids 165 (2022) 110699, https://doi.org/10.1016/j.jpcs.2022.110699.
[95] A. Nasser, M.A. Migahed, N.M. EL Basiony, H.M. Abd-El-Bary, T.A. Mohamed, Electrochemical, surface analysis, computational and anticorrosive studies of novel di-imine Schiff base on X65 steel surface, Sci. Rep. 13 (1) (2023) 17, https://doi.org/10.1038/s41598-023-37321-8.
[96] H.A. Mohamedien, S.M. Kamal, M. Taha, M.M. EL-Deeb, A.G. El-Deen, Experimental and computational evaluations of cefotaxime sodium drug as an efficient and green corrosion inhibitor for aluminum in NaOH solution, Mater. Chem. Phys. 290 (2022) 126546, https://doi.org/10.1016/j.matchemphys.2022.126546.
[97] C. Verma, H. Lgaz, D.K. Verma, E.E. Ebenso, I. Bahadur, M.A. Quraishi, Molecular dynamics and Monte Carlo simulations as powerful tools for study of interfacial adsorption behavior of corrosion inhibitors in aqueous phase: A review, J. Mol. Liq. 260 (2018) 99–120, https://doi.org/10.1016/j.molliq.2018.03.045.
[98] A. Rahimi, A. Farhadian, A. Berisha, A. Shaabani, M.A. Varfolomeev, V. Mehmeti, X. Zhong, S. Yousefzadeh, R. Djimasbe, Novel sucrose derivative as a thermally stable inhibitor for mild steel corrosion in 15% HCl medium: An experimental and computational study, Chem. Eng. J. 446 (2022), https://doi.org/10.1016/j.cej.2022.136938.
[99] I. Dehri, M. Erbil, Organic sulphur-containing compounds as corrosion inhibitors for mild steel in acidic media, Correl. Inhib. Effic. Chem. Struct. 236 (2004) 155–164, https://doi.org/10.1016/j.apsusc.2004.04.017.
[100] R. Solmaz, Investigation of the inhibition effect of 5- ((E) -4-phenylbuta-1, 3-dienylideneamino) - 1, 3, 4-thiadiazole-2-thiol Schiff base on mild steel corrosion in hydrochloric acid, Corros. Sci. 52 (2010) 3321–3330, https://doi.org/10.1016/j.corsci.2010.06.001.
[101] M. Mobin, R. Aslam, Experimental and theoretical study on corrosion inhibition performance of environmentally benign non-ionic surfactants for mild steel in 3. 5% NaCl solution, Process Saf. Environ. Prot. 114 (2013) 279–295, https://doi.org/10.1016/j.psep.2018.01.001.
[102] A. Singh Y. Lin K.R. Ansari M.A. Quraishi E.E. Ebenso S. Chen W. Liu Appl. Surf. Sci. Electrochem. Surf. Stud. some Porphines Corros. Inhib. J55 Steel sweet Corros. Environ. 359 2015 331 339.
[103] N.M. El Basiony, E.H. Tawfik, M.A. El-raouf, A.A. Fadda, M.M. Waly, Synthesis, characterization, theoretical calculations (DFT and MC), and experimental of different substituted pyridine derivatives as corrosion mitigation for X-65 steel corrosion in 1M HCl, J. Mol. Struct. 1231 (2021), https://doi.org/10.1016/j.molstruc.2021.129999.
[104] S.A. Haladu, N. Dalhat, S.A. Ali, A.M. Elsharif, N.A. Odewunmi, H.M.A. El-lateef, Inhibition of mild steel corrosion in 1 M H 2 SO 4 by a gemini surfactant 1, 6-hexyldiyl-bis- (dimethyldodecylammonium bromide): ANN, RSM predictive modeling, quantum chemical and MD simulation studies, J. Mol. Liq. 350 (2022) 118533, https://doi.org/10.1016/j.molliq.2022.118533.
[105] N.M. El Basiony, A. Nasser, E. Hafez, A. Elaraby, S.H. Shafek, A.H. Elged, D. Hwan, S.M. Shaban, Retard the corrosion reaction of carbon steel in acid solutions using Gemini-nonionic surfactant: theoretical and experimental studies, Mater. Today Commun. 37 (2023) 107378, https://doi.org/10.1016/j.mtcomm.2023.107378.